JOURNAL OF PETROLOGY | VOLUME 40 | NUMBER 3 | PAGES 475–494 | 1999

Steady-state Mantle–Melt Interactions in One Dimension: I. Equilibrium Transport and Melt Focusing

P. D. ASIMOW* AND E. M. STOLPER

DIVISION OF GEOLOGICAL AND PLANETARY SCIENCES, CALIFORNIA INSTITUTE OF TECHNOLOGY, PASADENA, CA 91125, USA

RECEIVED DECEMBER 1, 1997; REVISED TYPESCRIPT ACCEPTED AUGUST 13, 1998

Mantle–melt interaction during melt transport is explored in one dimension and steady state. We reconsider the equivalence between one-dimensional steady equilibrium transport and batch melting. In the absence of diffusion and radioactivity, conservation of mass flux requires that the major and trace element compositions of melt and solid at each point are the same as is generated by batch melting the source composition at the same pressure and temperature. Energy conservation requires that temperature and extent of melting are independent of melt migration except for irreversible source terms related to viscous compaction and gravitational energy release. The equivalence of phase compositions at each pressure between steady-state equilibrium transport and batch melting simplifies melt transport calculations. We examine the effects of increasing the melt flux to simulate melt focusing by channeling or by two-dimensional flow with converging melt streamlines. Melt focusing modifies the mineralogy of both residual matrix and erupted melt. We use MELTS calculations to model the formation of dunite by this mechanism and quantify the melt flux required to exhaust orthopyroxene from the residue as a function of pressure. The model dunites are found to be similar to natural dunites observed in the mantle section of ophiolite sequences.

KEY WORDS: *dunite; magma migration; porous flow; mid-ocean ridge processes*

INTRODUCTION

It is well established that on the time scale of pressure-release melting of the Earth's mantle, the liquid phase generally moves relative to the residual solid phases. This follows from experimental and theoretical studies of the equilibrium textures of olivine-dominated, partially molten systems, which indicate that the liquid phase is interconnected at melt fractions <1% (Waff & Bulau, 1979; von Bargen & Waff, 1986; Kohlstedt, 1991), suggesting that even at very low melt fractions, melt can begin to move by porous flow, driven by density differences or by shear of the matrix (McKenzie, 1984; Richter & McKenzie, 1984; Spiegelman & McKenzie, 1987; Stevenson & Scott, 1991). For reasonable grain sizes and rates of solid-state diffusion in the residual minerals, the expected rates of grain-scale porous flow are such that the moving melt is expected to approach closely equilibrium with the matrix minerals (Navon & Stolper, 1987; Spiegelman & Kenyon, 1992).

There is, however, considerable evidence that erupted mid-ocean ridge basalts (MORBs) are not in major or trace element equilibrium with typical lherzolite and harzburgite mantle residues at low pressure (O'Hara, 1968; Stolper, 1980; Johnson *et al.*, 1990), suggesting that erupted magmas contain at least a component of melts that did not stay in intimate contact with residual peridotites all the way to the top of the upper mantle. Furthermore, the time scale on which basalts are isolated from equilibration with the source and erupted is short compared with the half-life of daughter products in the decay series of ^{238}U (i.e. 1·5–100 kyr, Condomines *et al.*, 1981; Newman *et al.*, 1983; Reinitz & Turekian, 1989). Both of these lines of evidence suggest that not all of the melt produced under mid-ocean ridges is transported all the way from depth to the crust by diffuse porous flow

*Corresponding author. Present address: Lamont–Doherty Earth Observatory, Columbia University, PO Box 1000, Rt. 9W, Palisades, NY 10964, USA. Telephone: (914)365-8712. Fax: (914)365-8155. e-mail: asimow@ldeo.columbia.edu

and that there must be mechanisms for rapid extraction and transport of melt from depth. Proposed mechanisms for such rapid extraction and transport include: high-porosity regions formed by shear instability (Stevenson, 1989), reactive infiltration (Aharonov *et al.*, 1995; Kelemen *et al.*, 1995*b*), or steepening of propagating porosity waves (Scott & Stevenson, 1984; Spiegelman, 1993*a*, 1993*b*); open channels formed by diking (Sleep, 1988); or a fractal hierarchy of melt pathways (Hart, 1993).

In this paper, we explore the effects of increasing melt flux in a region of focused melt flow given complete thermal and chemical equilibrium between the melt and the solid in a high-porosity channel. Our treatment utilizes calculations based on the MELTS package of models and algorithms for equilibrium calculations in silicate systems (Ghiorso, 1994; Ghiorso & Sack, 1995). Within the internally consistent framework of MELTS, the complete phase equilibria and energetics of arbitrary bulk compositions in multicomponent systems can be calculated. It thus permits computation of effects (Asimow *et al.*, 1995, 1997) that generally are not accessible to calculation based only on direct parameterizations of experimental phase equilibrium data (Klein & Langmuir, 1987; McKenzie & Bickle, 1988; Niu & Batiza, 1991; Kinzler & Grove, 1992; Langmuir *et al.*, 1992) and that have previously been dealt with only by relatively simple thermodynamic treatments (Turcotte & Ahern, 1978; McKenzie, 1984; Hess, 1992). Earlier versions of MELTS (i.e. SILMIN) have been applied to the equilibrium porous flow problem (Kelemen & Ghiorso, 1986; Kelemen, 1990; Kelemen *et al.*, 1992), treating the process as one of isobaric assimilation at either fixed temperature or fixed enthalpy. Improvements in the MELTS models and algorithms, together with the concept of the formal equivalence of this problem to batch melting (developed below), allow us to calculate the entire one-dimensional upwelling system. This one-dimensional calculation is better suited to characterizing the evolution of the residual mantle column in space and time as a function of increasing melt flux than the approach of Kelemen (Kelemen & Ghiorso, 1986; Kelemen, 1990; Kelemen *et al.*, 1997), which focused on the evolution of a single parcel of liquid assimilating progressively larger amounts of peridotite.

Although melt flow beneath mid-ocean ridges is at least two-dimensional (Ahern & Turcotte, 1979; Phipps Morgan, 1987; Spiegelman & McKenzie, 1987) and probably includes a significant component of three-dimensional flow (Phipps Morgan & Forsyth, 1988; Parmentier & Phipps Morgan, 1990; Sparks & Parmentier, 1993), one-dimensional calculations provide a simple and useful framework for thinking about more complicated flow regimes. A one-dimensional model of focused porous flow simulates the effects of higher-dimensional flows, the effects of which are essentially to add extra melt flux to a predominantly vertical axial flow. Finally, although there is no reason, *a priori*, to expect that melt extraction is a steady process (Scott & Stevenson, 1989), steady solutions of the sort we present provide a simple baseline for understanding time-dependent behaviors and may provide insight into the average behavior of a time-dependent system averaged over many fluctuations.

EQUILIBRIUM POROUS FLOW

We develop here a more general version of Ribe's (1985) proof that, in a steady-state, one-dimensional, ascending column undergoing melting and equilibrium porous flow, the extent of melting and the composition of both residue and melt (but not the amount of melt present and so not the bulk composition) are independent of the melt migration rate and therefore equivalent to that produced by batch melting (i.e. to the case of no melt migration). Ribe stated that this was an approximate result. We will examine the conditions under which this is an exact result (Spiegelman & Elliott, 1993; Spiegelman, 1996). Specifically, we will show that at equilibrium and steady state in one dimension and in the absence of diffusion along the flow direction, at any point in the column the liquid and solid have compositions that are the same as would be obtained at the same pressure, P, and temperature, T, by batch melting of the source composition entering the base of the column. For trace elements the partitioning of which is independent of P and T, only the extent of melting, F, need be specified and the porous flow system will yield the same phase compositions as batch melting of the source to the given F. For major elements or trace elements with variable partition coefficients, however, two of the three variables P, T, and F must be specified. The relationship between these variables can depend on the details of the one-dimensional column; however, once two of these variables are specified, the compositions of the coexisting phases will correspond to batch melting of the source at the same conditions. Furthermore, except for irreversible source terms (related to gravity and viscous deformation of the solid), conservation of energy in the one-dimensional, steady-state, equilibrium porous flow system reduces to the same P–T–F path as isentropic (i.e. adiabatic and reversible) batch melting. This means that when these source terms are neglected, then even for elements (major or trace) with variable partition coefficients, only one of the variables, P, T, and F, needs to be specified and the liquid and solid compositions are the same as those obtained by isentropic batch melting of the source composition from the same initial potential temperature. Nevertheless, even when the dissipative source terms in the energy equation are non-zero, the steady equilibrium porous flow system still is restricted to liquid and solid

compositions consistent with batch melting, although in this case the path through *P–T–F* space is different and two independent variables must be specified to relate the compositions to batch melts and residues of the source composition.

The system we consider is illustrated schematically in Fig. 1a, where z is the vertical distance measured upwards from the bottom of the column. A one-dimensional isentropic column of solid mantle moving upwards with velocity $W(z)$ intersects its solidus at z_o, at which point its velocity is W_o. Once melt begins to form at this depth, it moves at velocity $w(z)$. As melting proceeds, the mass fraction of the solid residue that has been melted (which we refer to as the extent of melting, F) can be defined using the concentration of a perfectly compatible tracer (*pct*) in the residue: $F(z) \equiv 1 - X_o^{pct}/X_s^{pct}(z)$, where X_o^{pct} is the concentration in the initial bulk solid before melting begins and $X_s^{pct}(z)$ is the concentration in the bulk solid residue at some depth z (Scott, 1992; Spiegelman, 1996). It should be noted that because of the relative motions of solid and liquid, the porosity (i.e. the fraction of the volume that is occupied by liquid at any depth, φ) does not necessarily bear any simple relationship to F except in the case where the liquid is not permitted to move relative to the solid (i.e. if $w = W$, which is batch melting, in which case $F = \varphi\rho_f/[\varphi\rho_f + (1-\varphi)\rho_s]$). Although both F and φ have sometimes been termed the 'melt fraction' in the literature [e.g. both usages appear in McKenzie (1984)], it is critical here and elsewhere to distinguish clearly between them. In the most general case, where arbitrary liquids might be added or removed from a system, it might no longer be meaningful to call F the 'extent of melting', but in all cases it can be defined as above and retains a definite physical meaning; i.e. one minus the mass of the solid in the residue divided by the original solid mass, which in the frame of reference traveling with the solid is the fraction of the original solid mass that has been melted. Our first task is to show under what conditions $F(z)$ and the compositions of coexisting solid and liquid do not depend on $w - W$ or φ.

Mass flux

We begin in the same manner as McKenzie (1984), Ribe (1985), and Richter (1986) by stating the conservation of the mass of each component in the melt and the matrix, respectively:

$$\frac{\partial}{\partial t}\left[\varphi\rho_f X_f^n\right] + \frac{\partial}{\partial z}\left[\varphi\rho_f X_f^n w\right] = \Gamma^n \quad (1)$$

$$\frac{\partial}{\partial t}\left[(1-\varphi)\rho_s X_s^n\right] + \frac{\partial}{\partial z}\left[(1-\varphi)\rho_s X_s^n W\right] = -\Gamma^n \quad (2)$$

where t is time, ρ is density, the subscripts f and s refer to melt and solid (the solid assemblage may be polymineralic, but all solid phases move at the same velocity so only bulk properties of the solid assemblage are needed), X_f^n and X_s^n are the concentrations in mass units of the nth component in our N-component system in the melt and solid (normalized so that $\sum_{n=1}^{N} X_f^n = \sum_{n=1}^{N} X_s^n = 1$), and Γ^n is the rate of mass transfer of the nth component from matrix to melt. At steady state,

$$\frac{\partial}{\partial z}\left[\varphi\rho_f X_f^n w\right] = \Gamma^n \quad (3)$$

$$\frac{\partial}{\partial z}\left[(1-\varphi)\rho_s X_s^n W\right] = -\Gamma^n. \quad (4)$$

Adding (3) to (4) and integrating from z_o to z subject to the boundary conditions $\varphi(z_o) = 0$, $\rho_s(z_o) = \rho_s^o$, $X_s^n(z_o) = X_o^n$, and $W(z_o) = W_o$ yields

$$\varphi\rho_f X_f^n w + (1-\varphi)\rho_s X_s^n W = \rho_s^o X_o^n W_o. \quad (5)$$

Summing the equivalent of equation (5) for each component from one to N gives a constraint on the total mass flux:

$$\varphi\rho_f w + (1-\varphi)\rho_s W = \rho_s^o W_o. \quad (6)$$

At this stage, Ribe (1985) assumed constant ρ_s and a two-component system with a single compositional variable. We proceed for the general N-component, variable density case. Eliminating w between (5) and (6) and introducing the definition for each component $F^n = (X_o^n - X_s^n)/(X_f^n - X_s^n)$, we obtain

$$(1-\varphi)\rho_s W = (1-F^n)\rho_s^o W_o \quad (7)$$

and eliminating W between (5) and (6) we likewise obtain

$$\varphi\rho_f w = F^n \rho_s^0 W_o. \quad (8)$$

As φ, ρ_f, ρ_s, ρ_s^o, w, W, and W_o are the same for all N components, equations (7) and (8) show that F^n has the same value when defined using any component, including a perfectly compatible tracer (for which $X_f^{pct} = 0$, so that $F^{pct} = F$ as defined above). This is a simple but key result: at steady state in one dimension, all components give the same 'extent of melting' as originally defined above based on a perfectly compatible tracer. Hence we can simply use F in place of F^n for all elements, so

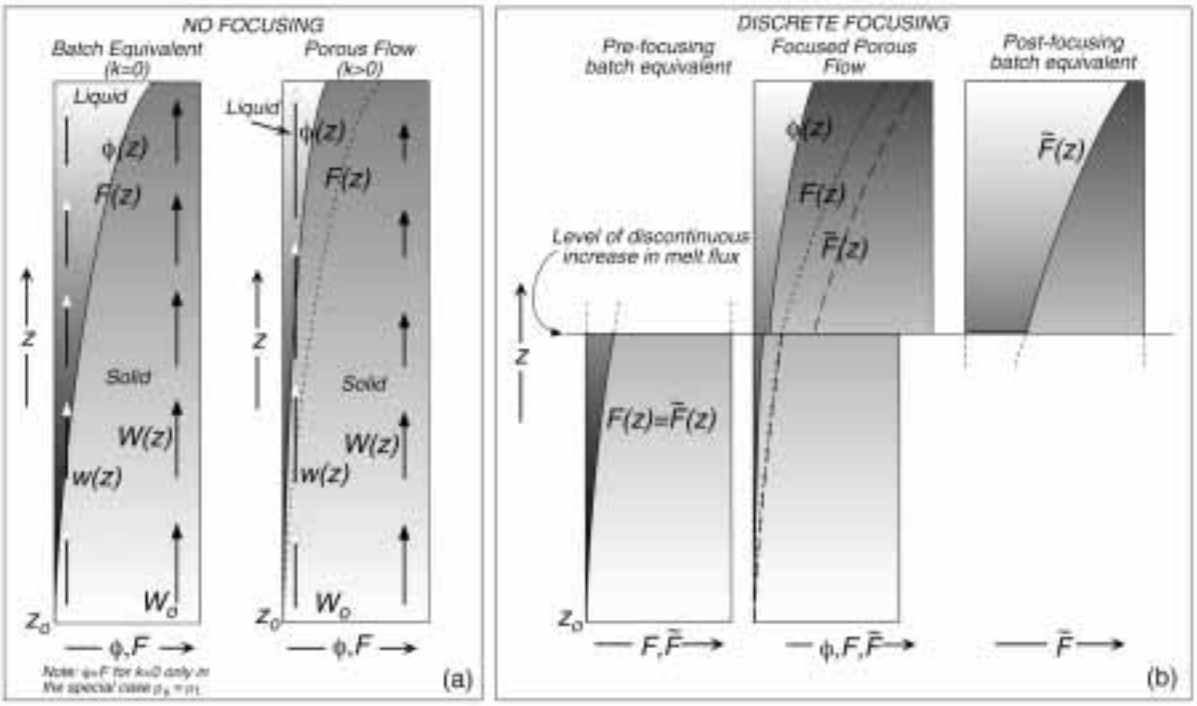

Fig. 1. Schematic representations of steady one-dimensional equilibrium porous flow columns. All diffusion is neglected; except for irreversibility associated with relative motion of liquid and solid, the system is isentropic. The vertical coordinate, z, increases upwards from z_o at the bottom, which is the depth at which the adiabat intersects the solidus and melting begins. The fraction of liquid by volume, $\varphi(z)$, is represented by the width of the 'liquid' field as a fraction of the width of the column. The extent of melting, $F(z)$, is represented schematically by the concentration of a perfectly compatible tracer in the solid (stippling in the solid field) and is also plotted as a short-dashed line for the special case $\rho_s = \rho_f$ (this special case is assumed only for this figure, not in the text or calculations; note that F is a mass fraction and φ is a volume fraction). The composition of the liquid is indicated schematically by the concentration of a perfectly incompatible element (shading in the liquid field). The vertical velocity of the solid, $W(z)$, is shown by black-headed arrows and at z_o is equal to W_o. The vertical velocity of the liquid, $w(z)$, (shown by white-headed arrows) is controlled by Darcy's law. (a) This illustrates schematically the equivalence proved in the first section of the text; it compares the case of batch melting on the left (i.e. permeability, k, is zero, $W=w$ and $\varphi=(F/\rho_f)/[(F/\rho_f)+(1-F)/\rho_s]$ everywhere; W is in general not constant because densities are functions of pressure) with the case of equilibrium porous flow on the right (a non-zero k which is an increasing function of φ, hence $w > W$ and increases upwards). For the porous flow case on the right, conservation of mass flux requires that $\varphi<(F/\rho_f)/[(F/\rho_f)+(1-F)/\rho_s]$ (i.e. $\varphi < F$ for $\rho_s = \rho_f$) as $w > W$, but F and the composition of liquid and solid do not depend on k, φ, or w (hence the F curve and the shadings are identical in the left and right columns). The vertical fluxes of each component and of entropy are the same in the porous flow and equivalent batch melting systems. (b) This illustrates the use of the equivalence shown in (a) to model a 'discrete' melt focusing event (see Fig. 2): to simulate the addition of extra melt flux to the column at a particular depth, we choose a new equivalent batch melting column by tuning the bulk composition and entropy until the fluxes match the desired values. The half-column on the left shows the equivalent batch melting column before focusing, the full column in the middle represents the porous flow column with the focusing event, and the half-column on the right shows the new equivalent batch melting column after focusing. The quantity $\tilde{F}$ is used for the extent of melting in the equivalent batch melting column after focusing, because by definition F is referenced back to a perfectly compatible tracer in the pre-focusing batch melting equivalent. F is continuous through the focusing event with a sharp change in slope, whereas $\tilde{F}$ is discontinuous at the focusing event. The 'continuous' focusing calculation (Figs 4–7) iterates this operation of substituting a new equivalent batch melting column many times.

$$(1-\varphi)\rho_s W=(1-F)\rho_s^o W_o \qquad (7')$$

$$\varphi\rho_f w=F\rho_s^o W_o. \qquad (8')$$

The relationship between F, Γ^n, and the total mass transfer between solid and liquid, Γ, follows from equating the partial derivative of (7′) with respect to z with the sum of all N equations (4) (recall that $\sum_{n=1}^{N} X_s^n = 1$):

$$\Gamma \equiv \sum_{n=1}^{N} \Gamma^n = \rho_s^o W_o \frac{\partial F}{\partial z}. \qquad (9)$$

We are now in a position to show that given certain assumptions, various characteristics of the melting column are independent of w, W, and φ; i.e. they do not depend on the amount of melt present or the rate of melt migration.

Major elements

If we substitute (7′) and (8′) into (5) we obtain the central result of this section,

$$FX_f^n+(1-F)X_s^n=X_o^n \quad (10)$$

i.e. the mass flux constraints require all elements to be partitioned in a manner that depends only on F and not on φ. In other words, even though the bulk composition of the column (i.e. $\varphi\rho_f X_f^n+(1-\varphi)\rho_s X_s^n$) varies with depth and depends on φ, the effective bulk composition that governs equilibration even of major elements at all depths in the column is given by $FX_f^n+(1-F)X_s^n=X_o^n$. As (10) is the governing equation for batch fusion, the compositions of melt and bulk solid are the same at each point in the column as would be obtained by batch fusion of the source composition at the same P and T (or the same P and F, or the same T and F, as only two of these three variables are independent), even if melt and solid are moving differentially. It may seem strange that the compositions of the phases at a given P and T are the same in the steady-state porous flow and batch fusion cases, as the bulk compositions (i.e. of the solid plus liquid assemblage) at these conditions differ for the two cases, but this is certainly a possible solution because one can change the amount of a phase present in a system at equilibrium without affecting the amounts or compositions of other phases and remain at equilibrium. This is in fact the unique solution given the requirements of steady state, one dimension, and local equilibrium (that is, exchange between liquid and solid is effectively infinite so that all chemical potentials are equal among phases at a given P or z, but diffusivity in the P or z direction is zero so that chemical gradients along the flow path have no effect). Hence, although the bulk composition (liquid plus residue) at any point in the column depends on the specific characteristics of melt transport (permeability, porosity, etc.), the composition of the liquid and of the solid residue taken separately do not.

Trace elements

A notable special case is the conservation of an element for which chemical equilibrium is expressed using a partition coefficient, $K^n=X_s^n/X_f^n$ (which need not be a constant; i.e. it can be an arbitrary function of P, T, modal proportions, liquid composition, and mineral composition). In this case, (10) takes the familiar form of trace element partitioning in batch melting,

$$\frac{X_f^n}{X_o^n}=\frac{1}{K^n+(1-K^n)F}. \quad (11)$$

This shows that the concentration of a stable, nonradiogenic trace element in the liquid (and hence in the solid) as a function of F is independent of solid velocity, liquid velocity, permeability, and porosity as long as equilibrium is maintained and the column is in steady state (Ribe, 1985; Richter, 1986; Spiegelman & Elliott, 1993). It should be noted that the assumption of steady state excludes chromatographic dispersion associated with the time-dependent propagation of trace-element fronts and gradients through an equilibrium porous flow system (Navon & Stolper, 1987).

Residual mode and mineral compositions

Although the above analysis was written using bulk solid residue composition and velocity, we could equally well have defined a separate composition and velocity for each phase in the solid residue, which would lead to the conclusion that the composition of each solid phase taken separately does not depend on the presence or parameters of melt transport. In the case we treat here, where all solid phases move at the same velocity, the fact that all the solid phase compositions as well as the total solid composition are each independent of melt transport requires that the same is true of the modal proportions of the solid phases. The result that both the proportions and compositions of the individual phases in the solid assemblage during one-dimensional steady-state equilibrium melt transport are identical to batch melting of the source composition will be used below to interpret melt-focusing calculations.

Entropy flux

For elements whose behavior is independent of temperature and pressure, the foregoing demonstrates that the concentrations in liquid and solid at each level in a one-dimensional column in local equilibrium and in steady state undergoing porous flow will be identical to those achieved for batch melting at the same F [equation (10)]. For elements with temperature- and pressure-dependent behavior (whether major elements or trace elements with variable partition coefficients), the compositions of the coexisting phases in the steady porous flow case can be determined from the results of simple batch melting calculations if two variables among F, P, and T are specified. Although batch melting can follow an arbitrary P–T path with F considered a dependent variable at equilibrium, in the particular case of isentropic (i.e. adiabatic and reversible) batch melting, F and T are both dependent variables [i.e. $F(P)$ and $T(P)$ are unique functions of P, given a value of the specific entropy of the system, or, equivalently, of the temperature at 1 bar of the metastable solid assemblage with the same bulk composition and specific entropy as the source, its 'potential temperature' (McKenzie & Bickle, 1988)] given the energetics of melting and reaction (Asimow *et al.*, 1997). The concentrations of major elements and trace elements with variable partition coefficients will be the same for the porous flow and isentropic batch melting cases at a given F or P only if the porous flow system obeys the $F(P)$ and $T(P)$ relations governing isentropic

batch melting. In this section we investigate the conditions under which this is the case by deriving expressions for melt productivity and temperature gradient in the steady-state, one-dimensional, equilibrium porous flow system.

McKenzie (1984) gave an equation for conservation of energy in a continuum containing solid and liquid with separate velocity fields but a common temperature and pressure [his equation (A36)] and used conservation of momentum and mass to convert to an entropy conservation equation (A37) that at steady state and in one dimension can be written

$$T(S_f-S_s)\Gamma + T(1-\varphi)\rho_s W\frac{dS_s}{dz} + T\varphi\rho_f w\frac{dS_f}{dz} = \frac{d}{dz}\left[k_T\frac{dT}{dz}\right] + \frac{\mu\varphi^2}{k}(w-W)^2 + (\zeta+\frac{4}{3}\eta)\left(\frac{dW}{dz}\right)^2 + H \quad (12)$$

where S_f and S_s are the specific entropies of the melt and matrix, k_T is the bulk thermal diffusivity, μ is the viscosity of the melt, k is the permeability, ζ is the bulk viscosity and η the shear viscosity of the matrix, and H is the rate of internal heat generation. McKenzie (1984) derived (12) using a treatment that is correct only for reversible processes in one-component systems, but the same equation results when multicomponent terms are taken into account provided that solid and liquid are homogeneous and in chemical equilibrium at each level in the column. The four terms on the right-hand side of (12) represent, respectively, the contributions of thermal diffusion, gravitational potential energy dissipated by viscous flow of the melt, dissipation by compaction of the solid, and internal heat generation (e.g. by radioactivity) to the change in internal energy of the system. In this treatment we neglect internal heat generation as well as thermal diffusion (i.e. we assume $H = 0$ and $k_T = 0$, such that in the further special case $w = W$, each unit volume evolves adiabatically).

Using (7′), (8′), and (9) and rearranging, we obtain

$$(S_f-S_s)\frac{dF}{dz} + (1-F)\frac{dS_s}{dz} + F\frac{dS_f}{dz} = \frac{1}{T\rho_s^o W_o}\left(\frac{\mu\varphi^2}{k}(w-W)^2 + \left(\zeta+\frac{4}{3}\eta\right)\left(\frac{dW}{dz}\right)^2\right). \quad (13)$$

Equation (13) can be used to find both the entropy of a steady-state column and its temperature as functions of P or z.

Entropy

To obtain entropy, we integrate (13) subject to boundary conditions $S_s(z_o) = S_s^o$ and $F(z_o) = 0$:

$$(FS_f + (1-F)S_s) = S_s^o + \frac{1}{\rho_s^o W_o}\int_{z_0}^{z}\frac{1}{T}\left(\frac{\mu\varphi^2}{k}(w-W)^2 + \left(\zeta+\frac{4}{3}\eta\right)\left(\frac{dW}{dz}\right)^2\right)dz. \quad (14)$$

This states that, except for the dissipative source terms given in the integral on the right-hand side, the system acts identically to the isentropic batch melting case, where $(FS_f + (1-F)S_s) = S_s^o$. This result is analogous to the results in the previous section for composition: for a given F, the specific entropies of liquid and solid, like the compositions of liquid and solid, are the same (in the absence of the source terms) for diffusion-free equilibrium porous flow and for isentropic (i.e. adiabatic and reversible) batch melting, even though the total entropy, like the bulk composition, may vary with depth in the porous flow case.

Temperature and melt productivity

To obtain an equation for temperature as a function of depth or pressure, we expand the total differentials of S_f and S_s,

$$dS_s = \frac{C_p^s}{T}dT - \frac{\alpha_s}{\rho_s}dP + \sum_{n=1}^{N} S_s^n dX_s^n = \frac{C_p^s}{T}dT - \frac{\alpha_s}{\rho_s}dP + \sum_{n=1}^{N} S_s^n\left(\left(\frac{\partial X_s^n}{\partial F}\right)_P dF + \left(\frac{\partial X_s^n}{\partial P}\right)_F dP\right), \quad (15a)$$

$$dS_f = \frac{C_p^f}{T}dT - \frac{\alpha_f}{\rho_f}dP + \sum_{n=1}^{N} S_f^n dX_f^n = \frac{C_p^f}{T}dT - \frac{\alpha_f}{\rho_f}dP + \sum_{n=1}^{N} S_f^n\left(\left(\frac{\partial X_f^n}{\partial F}\right)_P dF + \left(\frac{\partial X_f^n}{\partial P}\right)_F dP\right) \quad (15b)$$

where α_s is the isobaric coefficient of thermal expansion and C_p^s the isobaric heat capacity of the bulk solid assemblage, S_s^n is the partial specific entropy of component n in the bulk solid assemblage (encompassing both modal and compositional effects), and α_f, C_p^f, and S_f^n are the analogous properties for the liquid phase. We could also write the modal and compositional effects separately. If the solid assemblage consists of $\mathcal{J}$ solid phases, where phase j has modal mass fraction γ^j, specific entropy S^j, and $\mathcal{N}^j$ components with concentrations X_n^j and partial specific entropies S_n^j, then (15a) can be written

$$dS_s = \frac{C_p^s}{T}dT - \frac{\alpha_s}{\rho_s}dP + \sum_{j=1}^{\mathcal{J}}\left[S^j d\gamma^j + \gamma^j\sum_{n=1}^{\mathcal{N}^j} S_n^j dX_n^j\right].$$

After introducing the shorthand notations

$$\left(\frac{\partial S_X^s}{\partial P}\right)_F = \sum_{n=1}^{N} S_s^n \left(\frac{\partial X_s^n}{\partial P}\right)_F, \quad \left(\frac{\partial S_X^f}{\partial P}\right)_F = \sum_{n=1}^{N} S_f^n \left(\frac{\partial X_f^n}{\partial P}\right)_F$$

$$\left(\frac{\partial S_X^s}{\partial F}\right)_P = \sum_{n=1}^{N} S_s^n \left(\frac{\partial X_s^n}{\partial F}\right)_P, \quad \left(\frac{\partial S_X^f}{\partial F}\right)_P = \sum_{n=1}^{N} S_f^n \left(\frac{\partial X_f^n}{\partial F}\right)_P$$

for the compositional and modal entropy changes resulting from melting, summed over all components (Asimow *et al.*, 1997), (15) can be written

$$\mathrm{d}S_s = \frac{C_\mathrm{p}^s}{\mathcal{T}}\mathrm{d}\mathcal{T} + \left(\left(\frac{\partial S_X^s}{\partial P}\right)_F - \frac{\alpha_s}{\rho_s}\right)\mathrm{d}P + \left(\frac{\partial S_X^s}{\partial F}\right)_P dF \quad (16a)$$

$$\mathrm{d}S_f = \frac{C_\mathrm{p}^f}{\mathcal{T}}\mathrm{d}\mathcal{T} + \left(\left(\frac{\partial S_X^f}{\partial P}\right)_F - \frac{\alpha_f}{\rho_f}\right)\mathrm{d}P + \left(\frac{\partial S_X^f}{\partial F}\right)_P dF. \quad (16b)$$

Introducing these expansions into (13), together with the assumption of hydrostatic equilibrium, $\mathrm{d}P/\mathrm{d}z = g[\varphi\rho_f + (1-\varphi)\rho_s]$, gives

$$\mathcal{T}\left[(S_f - S_s) + \left(\frac{\partial S_X}{\partial F}\right)_P\right]\frac{\mathrm{d}F}{\mathrm{d}P} + \mathcal{T}\left[\left(\frac{\partial S_X}{\partial P}\right)_F - F\frac{\alpha_f}{\rho_f} - (1-F)\frac{\alpha_s}{\rho_s}\right] + [FC_\mathrm{p}^f + (1-F)C_\mathrm{p}^s]\frac{\mathrm{d}\mathcal{T}}{\mathrm{d}P} = \frac{1}{\rho_s^o W^o g[\varphi\rho_f + (1-\varphi)\rho_s]}\left(\frac{\mu\varphi^2}{k}(w-W)^2 + \left(\zeta + \frac{4}{3}\eta\right)\left(\frac{\mathrm{d}W}{\mathrm{d}z}\right)^2\right) \quad (17)$$

where

$$(\partial S_X/\partial P)_F = F(\partial S_X^f/\partial P)_F + (1-F)(\partial S_X^s/\partial P)_F,$$
$$(\partial S_X/\partial F)_P = F(\partial S_X^f/\partial F)_P + (1-F)(\partial S_X^s/\partial F)_P,$$

and $(S_f - S_s) + (\partial S_X/\partial F)_P$ is retained in place of the conventional but ill-defined substitution of ΔS_{fus} for this quantity (Asimow *et al.*, 1997; Hirschmann *et al.*, 1999). The terms on the left-hand side of (17) are due, respectively, to changes along the flow direction in melt fraction, pressure (i.e. adiabatic expansion), and temperature (i.e. thermal advection).

With the identity

$$\frac{\mathrm{d}\mathcal{T}}{\mathrm{d}P} = \left(\frac{\partial \mathcal{T}}{\partial F}\right)_P \frac{\mathrm{d}F}{\mathrm{d}P} + \left(\frac{\partial \mathcal{T}}{\partial P}\right)_F \quad (18)$$

we can solve (17) for the melt productivity, $-(\mathrm{d}F/\mathrm{d}P)$, and the temperature gradient, $(\mathrm{d}\mathcal{T}/\mathrm{d}P)$, separately. Substituting (18) into (17) and rearranging leads to

$$-\left(\frac{\mathrm{d}F}{\mathrm{d}P}\right) = \frac{\left(\frac{FC_\mathrm{p}^f + (1-F)C_\mathrm{p}^s}{\mathcal{T}}\left(\frac{\partial \mathcal{T}}{\partial P}\right)_F - \left(F\frac{\alpha_f}{\rho_f} + (1-F)\frac{\alpha_s}{\rho_s}\right) + \left(\frac{\partial S_X}{\partial P}\right)_F + \frac{\frac{\mu\varphi^2}{k}(w-W)^2 + \left(\zeta + \frac{4}{3}\eta\right)\left(\frac{\mathrm{d}W}{\mathrm{d}z}\right)^2}{\mathcal{T}\rho_s^o W^o g[\varphi\rho_f + (1-\varphi)\rho_s]}\right)}{\frac{FC_\mathrm{p}^f + (1-F)C_\mathrm{p}^s}{\mathcal{T}(\partial F/\partial \mathcal{T})_P} + \left[(S_f - S_s) + \left(\frac{\partial S_X}{\partial F}\right)_P\right]}, \quad (19)$$

which is identical to the productivity for isentropic batch melting except for the dissipative source terms at the end of the numerator (Asimow *et al.*, 1997). Substituting (19) back into (18) gives the temperature gradient:

$$\left(\frac{\mathrm{d}\mathcal{T}}{\mathrm{d}P}\right) = \frac{\left(\left[(S_f - S_s) + \left(\frac{\partial S_X}{\partial F}\right)_P\right]\left(\frac{\partial F}{\partial \mathcal{T}}\right)_P\left(\frac{\partial \mathcal{T}}{\partial P}\right)_F + \left(F\frac{\alpha_f}{\rho_f} + (1-F)\frac{\alpha_s}{\rho_s}\right) - \left(\frac{\partial S_X}{\partial P}\right)_F - \frac{\frac{\mu\varphi^2}{k}(w-W)^2 + \left(\zeta + \frac{4}{3}\eta\right)\left(\frac{\mathrm{d}W}{\mathrm{d}z}\right)^2}{\mathcal{T}\rho_s^o W^o g[\varphi\rho_f + (1-\varphi)\rho_s]}\right)}{\frac{FC_\mathrm{p}^f + (1-F)C_\mathrm{p}^s}{\mathcal{T}} + \left[(S_f - S_s) + \left(\frac{\partial S_X}{\partial F}\right)_P\right]\left(\frac{\partial F}{\partial \mathcal{T}}\right)_P}. \quad (20)$$

As the velocity and porosity appear only in the dissipative source terms, equations (19) and (20) demonstrate that, as for composition in equation (10), the productivity and temperature gradient and hence F and $\mathcal{T}$ at any pressure in a one-dimensional, steady-state, equilibrium porous flow system are independent of melt and solid velocity, porosity, and permeability except in the dissipation terms.

Hence, neglecting the dissipation terms, the productivity and temperature gradient for the porous flow case are the same as the isentropic batch melting problem with the same initial conditions. This is surprising in that (12) includes advective terms as well, but the constraint of one-dimensional, steady-state conservation of energy renders the net advection independent of melt migration rates. It should be noted that the solid dissipation term (i.e. for matrix compaction) depends on migration velocities, but is not in general strictly zero, even for batch melting with no melt migration; i.e. equation (6) demonstrates that W cannot be constant (i.e. the compaction rate $\partial W/\partial z$ is non-zero) unless the melt and solid densities are equal and constant (this reflects the fact that in one dimension with melt and solid having the same velocity, changes in W are the only means to accommodate changes in volume while conserving mass flux). Porous flow, however, in general requires substantially greater compaction rates than batch melting [consider equation (7′), which shows that, for small $\varphi \ll F$ and $\rho_s \sim \rho_s^o$, W must change in proportion to $(1 - F)$ to conserve mass], so we would normally expect compaction to be a much greater heat source when porous flow is occurring. When there is no porous flow, the gravity term is exactly zero (because $w = W$) and dissipation in the melt is negligible [i.e. the melt viscosity is so many orders of magnitude less than the solid viscosity that when solid and liquid move together, effectively all the dissipation is due to deformation of the solid; note that a large difference in viscosity between solid and liquid phases is an assumption in the derivation of (12)]. For the porous flow case, viscous dissipation because of shear flow in the melt remains negligible except that in the inertia-less formulation of McKenzie (1984), the effect of separation flow in a gravitational field is incorporated as dissipation in the melt.

In reaching expressions for $-(\mathrm{d}F/\mathrm{d}P)$ and $(\mathrm{d}T/\mathrm{d}P)$, we used the expression $\mathrm{d}P/\mathrm{d}z = g[\varphi\rho_f + (1-\varphi)\rho_s]$. The mechanical equilibrium because of overburden pressure given by this expression depends on the density of the overlying column, which in turn depends on how much melt it contains. Therefore, although equations (17), (19), and (20) show that the steady, one-dimensional, equilibrium porous flow system and the isentropic batch melting column have exactly the same F and T at a given P when the dissipation terms are ignored, this result does not hold exactly when expressed in distance (z) terms [i.e. $-(\mathrm{d}F/\mathrm{d}z)$ and $(\mathrm{d}T/\mathrm{d}z)$ depend on φ even in the absence of dissipation]. In this paper we usually use pressure as the vertical coordinate, as P is a significant thermodynamic parameter whereas z is not.

Summary

For the formal equivalence between melt and solid composition and extent of melting as a function of P in a one-dimensional, steady-state, equilibrium porous flow system and during isentropic batch melting of the same source at the same potential temperature [which implies that $-(\mathrm{d}F/\mathrm{d}P)$ and $(\mathrm{d}T/\mathrm{d}P)$ are the same in the two cases] to hold, the following set of assumptions taken together is sufficient: (1) no thermal or chemical diffusion along the flow direction in either solid or melt phases; (2) no radioactive heating or transmutation of the elements (Spiegelman & Elliott, 1993); (3) negligible heating by dissipation owing to compaction of the solid matrix; (4) negligible dissipation of gravitational potential energy owing to vertical separation of fluid and solid of different densities. If (1)–(4) are assumed, then F, T, and phase compositions (and relative solid phase proportions, but not φ) as functions of P are independent of the presence and characteristics of melt migration. Furthermore, relaxing assumptions (3) and (4) yields source terms only in the energy equation; mass is still conserved in the manner of batch melting. Hence steady-state melt migration in the absence of these last two assumptions explores a family of batch melting paths with the same bulk composition but P–T and P–F paths that differ from those of isentropic batch melting. In a forthcoming paper, we evaluate these sources of deviation from the isentropic case and their effects on the P–T and P–F paths of one-dimensional systems.

MELT FOCUSING

Although one-dimensional porous flow is unlikely in most natural settings, there are some two- and three-dimensional flows that can be treated approximately in one dimension. For example, at a mid-ocean ridge undergoing passive (plate-driven) flow, the streamlines of melt migration by porous flow can be focused towards the axis (Phipps Morgan, 1987; Spiegelman & McKenzie, 1987). The axis of the ridge can therefore be approximated by one-dimensional vertical porous flow, with melt added to the column at various levels above the depth at which melting begins. On a smaller scale, study of infiltration of porous media by reactive melts has led to the recognition of a fingering instability in which narrow channels of high porosity and melt flux develop (Aharonov *et al.*, 1995; Kelemen *et al.*, 1995*b*). This situation can be approximated by one-dimensional vertical flow with melt added to the column either continuously or discretely at level(s) above that at which melting begins.

In this section, we use the formal equivalence of one-dimensional steady equilibrium porous flow to batch melting developed above to model melt focusing. By using this approach, we avoid the need to perform a simultaneous advection and equilibration calculation. Instead, each time melt is added to the system, the

problem is reduced to finding the equivalent set of independent variables (bulk composition and entropy or potential temperature) that when batch melted at the pressure of interest yields the new, higher melt-flux assemblage; neglecting the energy source terms discussed above, the phase compositions and the modal abundance of each solid phase in the residue will be the same in the focused porous flow situation and in the suitably chosen batch melting calculation. Just as for the general case above, there is no reason *a priori* to assume that the natural process will evolve to a steady state, but the steady calculation is simple and is a useful first step for interpreting any time-dependent model results.

In what follows, in the context of model results we use the term harzburgite to refer to model residues that are orthopyroxene (opx) bearing but clinopyroxene (cpx) free and dunite for model residues that are free of both opx and cpx. This usage, placing the boundaries between lherzolite, harzburgite, and dunite at zero modal abundances of opx and cpx, differs from standard petrographic nomenclature, which places the boundaries at 5% or 10% of these phases.

Discrete focusing

The case of a single focusing event, where melt flux is increased in the column at a single pressure, is the simplest to visualize (Fig. 1b). To illustrate, we consider a one-dimensional column undergoing isentropic upwelling that begins with the primitive upper-mantle source composition of Hart & Zindler (1986). For this particular example, with a potential temperature of 1300°C, the solidus is encountered at 1·9 GPa according to MELTS. At 1·0 GPa, we increase the melt flux by an arbitrary factor. In effect, a horizontal 'pipe' delivers, at a higher but still steady flux, melt from neighboring columns with the same composition and temperature as the melt already present. The 'focusing factor', Ω_D (D for discrete), in this case is just the ratio of melt flux infinitesimally above this level to that infinitesimally below it (we could also study neighboring columns that are depleted of melt by examining Ω_D values less than one). The trick that we perform to model the steady column at levels shallower than the focusing event is to find the bulk composition and entropy of the batch melting column equivalent to the new, higher-flux conditions; as described in the previous sections, by equivalent we mean that the fluxes of all chemical components and entropy are equal in the new batch melting column and in the equilibrium porous flow column after addition of melt flux. An increase in melt flux by a factor of Ω_D corresponds to an increase in the quantity of melt in the batch melting equivalent at this level by the same factor; the bulk composition and entropy of the batch melting equivalent above the level of focusing can then be calculated by simply adding the increased quantity of melt to the unchanged quantity of solid. It should be noted that permeability is some function of porosity, so the focusing event changes both φ and w at all higher levels in the column in a manner dependent on the particular permeability law we use; although φ and w depend on the permeability law, it should be emphasized that the P–T path and the compositional characteristics of solid and liquid at each level in the column after the focusing event are independent of the permeability law.

For a range of values of Ω_D, pressure is plotted against the calculated modal abundances of olivine and pyroxenes as mass fractions of the solid residue in the melting column in Fig. 2a and b. As the focusing event is at 1·0 GPa and changes only the amount of liquid, not the mode or composition of the residue at this point, all curves in Fig. 2a and b converge at this point. In the reference case ($\Omega_D = 1$, corresponding to no melt focusing) modal olivine increases to 77% of the residue at 1 bar, whereas opx initially increases by a small amount and then decreases, and cpx decreases (almost linearly as a function of melt fraction F, Fig. 2d). The slopes in Fig. 2d reflect the stoichiometry of the melting reaction (Baker & Stolper, 1994) calculated by MELTS for this bulk composition, which is cpx + spinel → olivine + opx + melt at high pressure and cpx + opx + spinel → olivine + melt at lower pressure until the exhaustion of cpx, after which the reaction is opx + spinel → olivine + melt. In the absence of focusing ($\Omega_D = 1$), cpx is calculated to be exhausted at 18% melting and 0·22 GPa, whereas opx remains in the residue throughout. To exhaust opx from the residue, it would be necessary to reach at least 36% melting, but even systems with substantially higher potential temperature than this example are unlikely to reach such a high extent of melting, because beyond the exhaustion of cpx, the melt productivity (Fig. 2c) is rather low (Hess, 1992; Langmuir *et al.*, 1992; Asimow *et al.*, 1997). This low melt productivity of harzburgite residues illustrated in Fig. 2c is the fundamental barrier to creation of dunite by simple decompression melting. As Ω_D increases, however, the rate of increase in modal olivine and decrease in modal pyroxenes at depths shallower than that at which melt is added increases sharply, such that above $\Omega_D = 6$, olivine and spinel are the only remaining phases at 1 bar. As Ω_D increases further, the pressure at which opx is exhausted increases, to about 0·3 GPa at $\Omega_D = 18$.

The reasons for accelerated exhaustion of opx in the case of melt focusing are simple to understand given the batch melting analogy developed above. We recall that although the physical situation envisaged is one of equilibrium porous flow with a focusing event, these calculations were performed as isentropic batch melting calculations. At the focusing event, the bulk composition

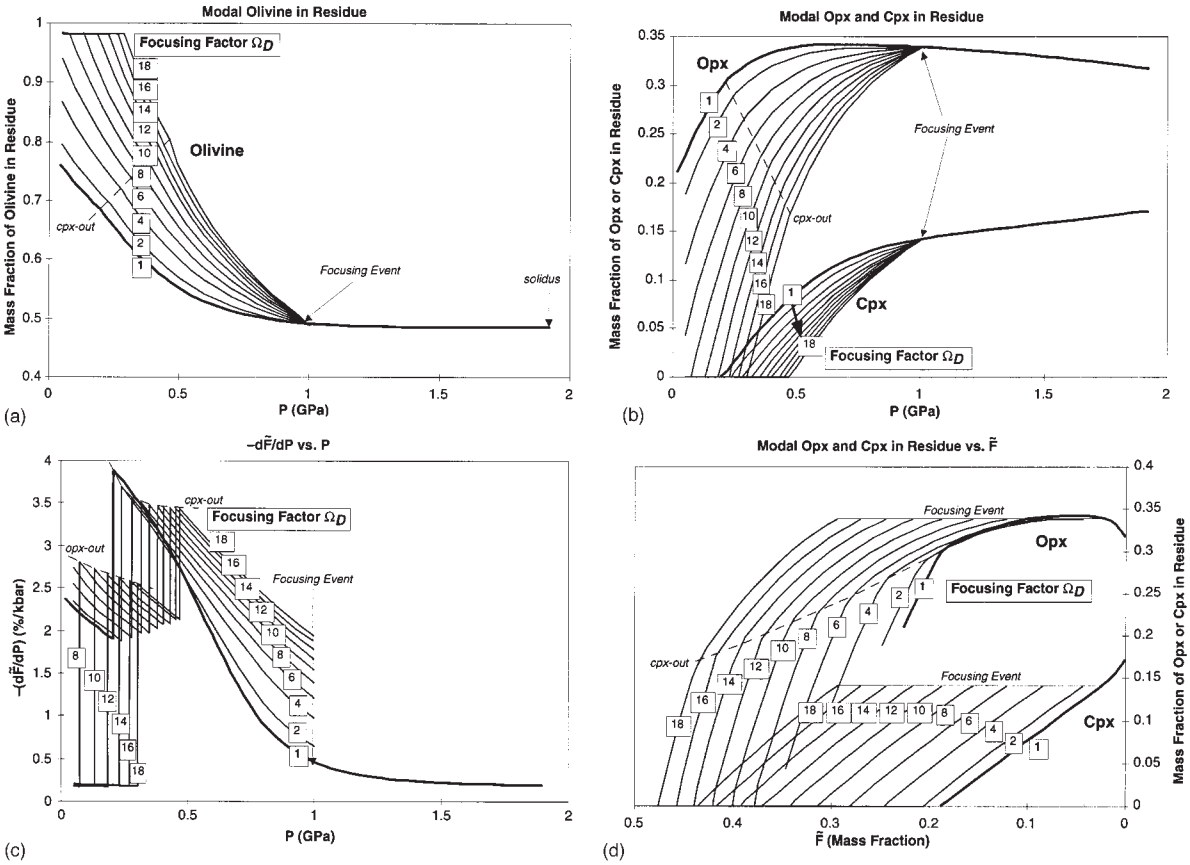

Fig. 2. The effect of a discrete focusing event that adds melt to a one-dimensional, steady, equilibrium porous flow column at 1·0 GPa. The source composition is the primitive upper mantle of Hart & Zindler (1986), including Cr_2O_3. The system begins melting at 1·9 GPa with initial mode 48% olivine, 32% orthopyroxene (opx), 17% clinopyroxene (cpx), and 3% spinel. (a) Mass fraction of olivine in the residual assemblage as a function of pressure (P); each curve at pressures lower than 1·0 GPa represents the olivine content of the residue vs pressure for a particular value of the focusing factor, Ω_D, the ratio of melt flux after focusing at 1·0 GPa to melt flux before focusing at 1·0 GPa. Modal olivine of ~0·98 indicates a dunite with ~2% spinel. The dashed line marks the exhaustion of cpx for each value of Ω_D. (b) Mass fractions of opx and cpx in the residual assemblage as functions of P. The focusing event at 1·0 GPa is indicated. The dashed line marks the modal abundance of opx at the exhaustion of cpx for each value of Ω_D. (c) Apparent melt productivity ($-d\tilde{F}/dP$) vs P. $\tilde{F}$ is the mass fraction of melt in the equivalent batch melting calculation, i.e. if the velocity of melt relative to solid is zero, $\tilde{F}$ is the mass fraction of melt actually present. As long as the residual phase assemblage remains the same, ($-d\tilde{F}/dP$) increases monotonically with Ω_D; productivity drops at the exhaustion of opx and cpx are indicated. (d) Mass fractions of opx and cpx in the residue plotted against $\tilde{F}$ on a reversed scale (i.e. the left ends of the opx curves represent 1 bar if opx remains in the residue at this pressure). The stoichiometric coefficient of cpx (slope on this diagram) in the melting reaction is roughly constant with respect to $\tilde{F}$ and Ω_D, whereas the coefficient of opx increases with $\tilde{F}$ and Ω_D. Hence less opx remains at the exhaustion of cpx (dashed line) for higher values of Ω_D.

and total entropy of the original source are replaced with those of the melt-enriched assemblage, and isentropic batch melting calculations on this assemblage are then used to model the characteristics of the shallower parts of the column. We can use the batch melting analogy to interpret the results as well as to execute the calculation. For most purposes in melt transport calculations, F is best taken as a property of the solid residue (measured, as described above, by the concentration of a perfectly compatible tracer), in which case F would be the same infinitesimally above and below the level of the focusing event at 1·0 GPa, as the solid composition does not change. In this calculation, however, it is instructive to use the melt fraction of the equivalent batch melting calculation, $\tilde{F}$ (i.e. one minus the mass fraction of solids in the new, melt-enriched system after focusing; see Fig. 1). $\tilde{F}$ is an apparent extent of melting, in that for both the porous flow case and the batch melting equivalent it equals the mass flux of melt divided by the total mass flux. The focusing event at 1·0 GPa immediately increases the melt flux by a factor of Ω_D and hence discontinuously increases $\tilde{F}$ (Fig. 2d).

When approached from the point of view of the equivalent batch melting column, the modal changes leading to the formation of dunite by melt focusing result from the sum of two effects that help to overcome the

barrier of the unproductive harzburgite region: (1) higher melt productivity, $-\mathrm{d}\tilde{F}/\mathrm{d}P$, in the batch melting system at each pressure; (2) changes in the stoichiometry of the lherzolite melting reaction that increase the coefficient for opx relative to melt while the coefficient for cpx remains roughly constant. The first effect, higher productivity, acts both in the harzburgite field (Fig. 2c), where it reduces the pressure drop between achievement of cpx exhaustion and opx exhaustion, and in the lherzolite field, where together with the roughly constant reaction coefficient for cpx it leads to exhaustion of cpx at higher pressure (which gives a larger pressure interval for harzburgite melting, Fig. 2b). The second effect leaves lower modal opx remaining at the exhaustion of cpx (dashed lines in Fig. 2b and d), which decreases both the increase in $\tilde{F}$ and the decrease in P required to traverse the harzburgite field. We explain each of these effects in the following paragraphs.

The reason $-\mathrm{d}\tilde{F}/\mathrm{d}P$ increases with increasing focusing in our calculations can be understood by analogy with a simple, isobaric phase loop in a two-component system (e.g. Fig. 3). The expression for batch isobaric productivity, $(\partial F/\partial T)_P$, in such a system (described by the end members a–b where a is the end member with the higher melting temperature) is:

$$\left(\frac{\partial F}{\partial T}\right)_P = -\left(\frac{\partial X_b^s}{\partial T}\right)_P \frac{1}{[X_b^f - X_b^s]} - \frac{F}{[X_b^f - X_b^s]}\left(\frac{\partial [X_b^f - X_b^s]}{\partial T}\right)_P \tag{21}$$

where X_b^f and X_b^s are the mass fractions of component b in the liquid and solid, respectively (Asimow *et al.*, 1997). The first term is independent of isothermal addition or subtraction of liquid to or from the system, but increasing F by adding liquid, moving the bulk composition closer to X_b^f, must increase the value of the second term [so long as $(\partial(X_b^f - X_b^s)/\partial T)_P$ is negative, which is always true for Mg-rich peridotites] and hence increase isobaric productivity. The relative contributions of the two terms in (21) and the effect of changing bulk composition are illustrated graphically in Fig. 3d. Because a higher isobaric productivity leads to a higher isentropic productivity (Asimow *et al.*, 1997), this simple analysis shows why the melt-enriched bulk compositions have enhanced productivity relative to the reference case ($\Omega_D = 1$), and by analogy why cpx and opx decrease in the mode at a given pressure with progressive melt-focusing. The increased $-\mathrm{d}\tilde{F}/\mathrm{d}P$ in the harzburgite field that accompanies higher Ω_D implies a decrease in the pressure drop, ΔP, required to achieve a given $\Delta\tilde{F}$; this acts together with the decrease in $\Delta\tilde{F}$ needed to exhaust opx (as less opx is present when cpx is exhausted, see below) to narrow the pressure range of harzburgite melting and to promote exhaustion of opx.

The same argument about productivity applies in the lherzolite melting field: as Ω_D increases this contributes to cpx exhaustion at higher pressure, which in turn leaves a wider pressure range over which to melt harzburgite, hence contributing to achieving a dunite residue by 1 bar (Fig. 2b and d). It should be noted that although with increasing Ω_D cpx persists to higher $\tilde{F}$ in our calculations (Fig. 2d), the stoichiometric coefficient for cpx in the polybaric melting reaction does not depend substantially on the bulk composition (reaction coefficients are represented by the slope of mass fraction of cpx vs $\tilde{F}$ curves in Fig. 2d), so the increase in $\tilde{F}$ *after focusing* required to exhaust cpx is similar for all values of Ω_D. However, as explained in the last paragraph, $-\mathrm{d}\tilde{F}/\mathrm{d}P$ is enhanced after focusing for higher values of Ω_D, so the increase in $\tilde{F}$ required to exhaust cpx from the residue is obtained over a smaller ΔP and so cpx exhaustion occurs at higher pressures for higher Ω_D.

The final factor in producing dunite residues is that (at least for this calculation) at higher focusing factors there is less opx remaining at the exhaustion of cpx, and thus that less melting in the relatively unproductive harzburgite field is required to produce dunite. This is due to a progressive change in the stoichiometry of the melting reaction with increasing focusing: as long as cpx remains in the residue, the mass of opx melted per unit change in $\tilde{F}$ increases with Ω_D (as illustrated by the increase in the slopes of the opx curves with Ω_D at the focusing event in Fig. 2d). As noted above, however, Fig. 2d also shows that the reaction coefficient for cpx does not change much either with Ω_D or with progressive upwelling for a particular Ω_D. The increase in reaction coefficient for opx together with the roughly constant coefficient for cpx means that although roughly the same increase in $\tilde{F}$ is required at all Ω_D to proceed from the focusing point to the exhaustion of cpx, the fraction of opx consumed over this range increases with Ω_D. Although the coefficient for opx after loss of cpx does not change significantly with increasing Ω_D, the smaller fraction of opx in the residue at cpx-out for the higher Ω_D cases means that a smaller increase in $\tilde{F}$ in the harzburgite field is required to reach a dunite residue. Furthermore, as explained above, $-\mathrm{d}\tilde{F}/\mathrm{d}P$ increases with Ω_D in the harzburgite field, so that the ΔP between cpx-out and opx-out decreases even faster with Ω_D than does the associated $\Delta\tilde{F}$.

Although we have not explored the degree to which the various aspects of these calculations can be generalized to other compositions and phase assemblages (but see below for the effect of focusing at different pressures), for this particular example the reaction coefficients for cpx are nearly constant along the melting path at fixed Ω_D and they are insensitive to changes in Ω_D, whereas both opx and olivine (not plotted, but the sum of coefficients for

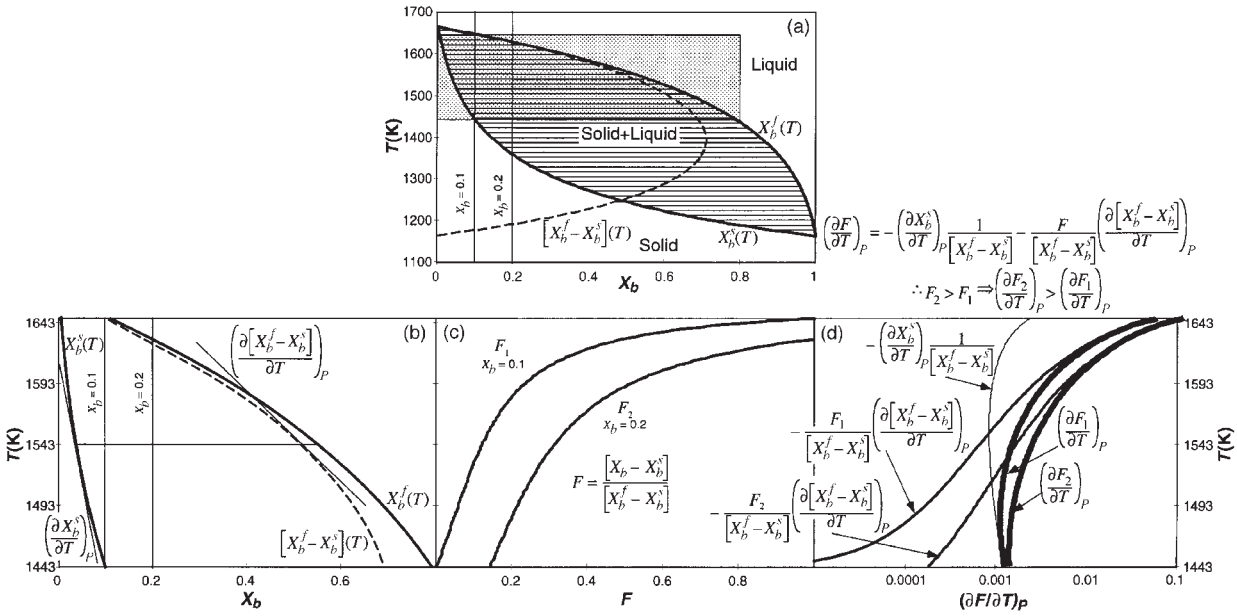

Fig. 3. Systematics of isobaric melt productivity in a binary phase loop. This simple example shows why higher extent of melting leads to higher melt productivity. (a) A hypothetical system *a–b* with ideal liquid and solid solutions and a difference in melting points at 1 bar of 500°C (Asimow *et al.*, 1997). The dashed curve plots the difference between liquid compositions and solid composition as a function of temperature. (b) Close-up of shaded area in (a) with derivatives $(\partial X_b^s/\partial T)_P$ and $(\partial(X_b^f - X_b^s)/\partial T)_P$ at 1543 K indicated by light tangent lines. (c) Temperature dependence of the extent of melting, F, for the two bulk compositions shown in (a) and (b) as given by the lever rule; composition 2, closer to the liquid composition than composition 1, has higher F at any given T. (d) Isobaric productivity, $(\partial F/\partial T)_P$, shown as the very heavy curves for compositions 1 and 2, is the sum of two terms as shown in the equation in the figure. The first term (light curve) is independent of F but the second term (moderately heavy curves) depends on F. In the region $T > 1414$ K where $(\partial(X_b^f - X_b^s)/\partial T)_P$ is negative, changing the bulk composition at constant temperature to give a higher F increases the value of the second term and yields a higher $(\partial F/\partial T)_P$.

opx, cpx, olivine, and spinel is constant) behave differently, with coefficients that change substantially along the melting path at fixed Ω_D and depend strongly on Ω_D. Furthermore, the direction in which each reaction coefficient changes with increasing Ω_D at fixed P is the same as the direction in which it changes with increasing $\tilde{F}$ at fixed Ω_D. It may at first seem surprising that the coefficients of the melting reaction change with Ω_D at the focusing point at 1·0 GPa even though all the phase compositions are the same at this point for all Ω_D. However, when melting is not taking place on a univariant curve (in which case the liquid and solid compositions are not uniquely specified at each pressure), there is no unique relationship between the instantaneous phase compositions and the melting reaction. In other words, during polybaric, high-variance melting of a nine-component system, the paths of the liquids in composition space and thus the reaction stoichiometries vary with bulk composition even at a point where all phases are identical in composition.

In summary, with increasing Ω_D the increase in productivity and the increase in the reaction coefficient for opx during lherzolite melting act together to promote the exhaustion of opx (and thus to produce dunite residues). A larger pressure range (ΔP) is available for harzburgite melting because cpx is exhausted at higher pressure, less melting ($\Delta\tilde{F}$) of harzburgite is required because less opx remains when cpx is exhausted, and the productivity ($-\mathrm{d}\tilde{F}/\mathrm{d}P$) is larger throughout. In some respects the results of Kelemen (1986, 1990) on dunite formation by isenthalpic assimilation of lherzolite into basaltic liquids are related to the results of this discrete focusing calculation. The calculated increase in productivity associated with adding liquid to the bulk composition that we describe here is related to Kelemen's conclusion that during isenthalpic assimilation of lherzolite by basaltic liquids, the mass of lherzolite assimilated is greater than the mass of olivine crystallized (i.e. the ratio $M_a/M_c > 1$) and so the mass of liquid increases. In other words, whether the generation of dunite residue is modeled by isentropic decompression of melt-enriched assemblages or the generation of liquid in equilibrium with dunite by isenthalpic, isobaric assimilation of peridotite into liquid, the end product is a system with more liquid than the initial lherzolite- or harzburgite-saturated systems. There does not appear to be any analogue of the change in opx and cpx reaction coefficients noted here in the work of Kelemen.

Continuous focusing

The foregoing analysis of a discrete focusing event leads naturally to a continuous focusing calculation, where a series of focusing events occurs as the system upwells. At fixed levels in the column (separated by small intervals in pressure), melt flux is increased by addition of melt of the same composition as that already in the column; at each such focusing event, a new bulk composition and total entropy of the equivalent batch melting system is then obtained as described above for the discrete focusing case and used to simulate the characteristics of the steady column until the level of the next focusing event. This procedure simulates a case where the flux of melt increases continuously upwards. The choice to add liquid of the same composition as that in the column at each level is somewhat arbitrary, but it is among the simplest of many possibilities; physically it can be envisioned as describing a scenario similar to that analyzed by Hart (1993), in which liquids contributed to the high-flux channel come from similar high-flux channels in a branching network. An equally simple alternative to be explored in future work would be to add liquids produced by fractional melting of the mantle adjacent to the channel rather than by equilibrium porous flow in neighboring channels. We consider here only the case where the incremental focusing events are evenly spaced in pressure and each has the same Ω_D value. The continuous focusing column is characterized by the integrated focusing factor $\Omega_I = \Omega_D{}^m$, where m is the number of incremental focusing events between the solidus and 1 bar. It should be noted that Ω_I is not equal to the factor by which the mass flux out of the top of the column exceeds the mass flux into the base of the column, because each focusing event increases the mass of liquid, not the mass of the system, by a factor Ω_D. Neither is Ω_I equal to the ratio of the melt flux from the top of the focused column to the melt flux in the reference case, as melt flux increases upwards in a steady-state column even without focusing (this ratio scales roughly as the square root of Ω_I). It is simply the product of focusing factors for all the discrete focusing events that are performed, and hence a measure of the total intensity of focusing.

The results of two continuous focusing calculations with solidus intersection pressures of 1·9 GPa and 3·5 GPa (initial potential temperatures before focusing begins of 1300°C and 1450°C, respectively) are shown in Figs 4 and 5. The reference case, $\Omega_I = 1$, for the colder example is the same one as used for the discrete focusing calculations and shown in Fig. 2. The effect of continuous focusing on the residual mode is seen to be similar to the single-focusing-event calculation—for values of Ω_I greater than one, modal olivine increases and modal pyroxenes decrease relative to the unfocused case. Above $\Omega_I = 4{\cdot}4$ for the cold case (and $\Omega_I = 2$ for the hot case), the residue is dunite (i.e. free of both opx and cpx) at 1 bar. The reasons for these modal changes are similar to the reasons for the corresponding behavior in the discrete focusing case: increased $-\mathrm{d}\tilde{F}/\mathrm{d}P$, related to increasing $\tilde{F}$ (Figs 4c and 5c; note that $-\mathrm{d}\tilde{F}/\mathrm{d}P$ in this case combines the extra melting effects between focusing events with the repeated discontinuous increases in $\tilde{F}$ at the focusing events), leading to exhaustion of cpx at higher pressure and more productive melting of harzburgite; together with increased reaction coefficient for opx with increasing $\tilde{F}$, reducing the quantity of opx remaining at the exhaustion of cpx (Figs 4d and 5d). The pressures at which the residue exhausts opx and cpx increase with Ω_I in a non-linear manner, as shown in Fig. 6: a small amount of focusing moves cpx-out and opx-out up a lot in pressure, but further focusing is subject to diminishing returns. For each potential temperature, there appears to be a practical upper limit to the pressure at which a dunite residue can be formed (about 0·5 GPa for a solidus at 1·9 GPa, about 0·8 GPa for a solidus at 3·5 GPa).

Discussion

The continuous focusing calculation is able to generate dunite residues, but only at rather low pressure. The limiting of opx-free residues to pressures <0·8 GPa in these calculations results from a convolution of two effects, one of which is a robust aspect of the described system and one of which is correct in sign but exaggerated by inaccuracies in MELTS. The robust basis for limitation of opx exhaustion to low pressure is, in part, the simple fact that melt flux increases upward by definition in the continuous focusing case, so the effects of focusing are enhanced at higher levels in the column; however, the thermodynamics of melting also play a role in that melt production and hence melt focusing are concentrated in the shallower parts of the melting regime because of the productivity function predicted by MELTS (Hirschmann *et al.*, 1994; Asimow *et al.*, 1997). If unlimited quantities of liquid were introduced at various depths, we could, of course, create dunites at higher pressures. In our calculations, however, melt focusing is coupled to melting, as we increase the melt flux by multiplicative factors relative to the melt flux in the column, rather than by arbitrary additive amounts. Focusing and its effects on the residue are therefore strongest at shallower levels where melt flux is already largest. Although the details are influenced by the particulars of our calculations, this general feature probably carries over into physically realistic melting regimes, where melt must be produced by decompression of adjacent columns before it can be focused into the column of interest. Moreover, at realistic potential temperatures for mid-ocean ridges (McKenzie & Bickle, 1988; Langmuir *et al.*, 1992), melt production

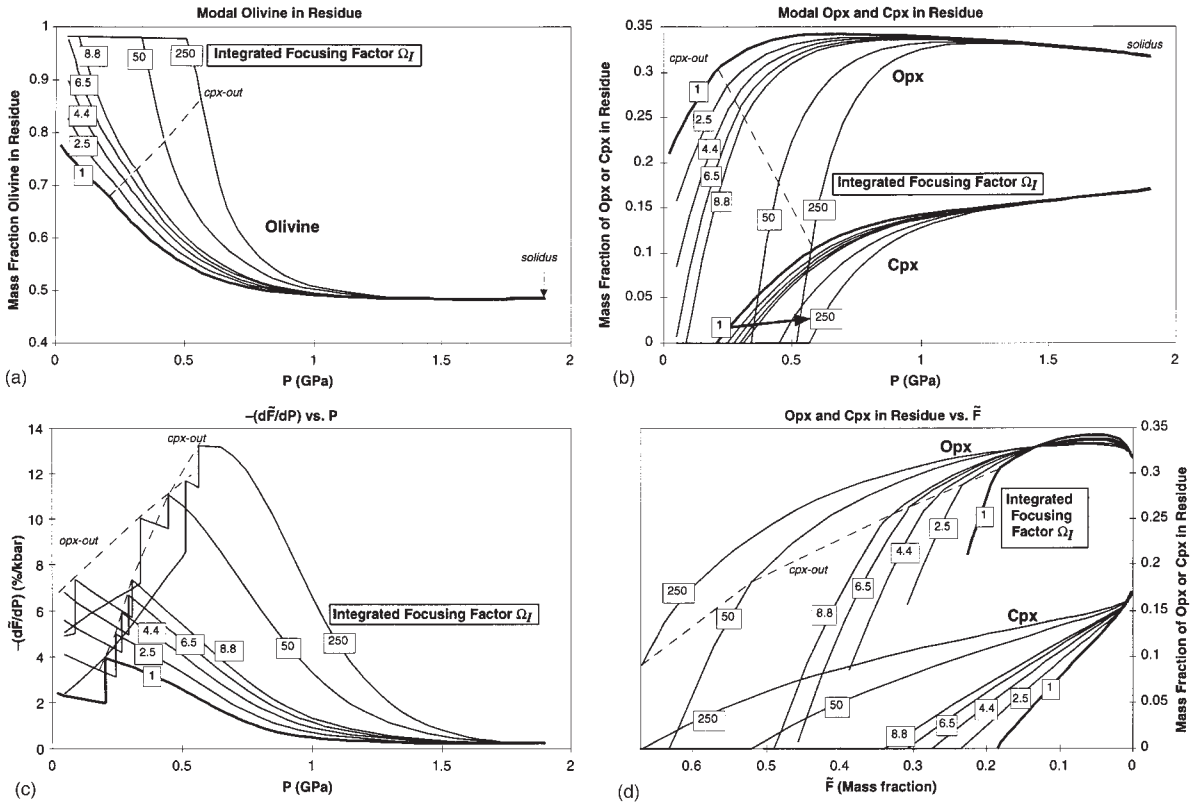

Fig. 4. The effect of continuous focusing of melt into a one-dimensional, steady, equilibrium porous flow column. The system begins melting at 1·9 GPa; every 50 MPa the melt flux is increased by a small factor. The product of all these incremental focusing factors over the entire column is the integrated focusing factor Ω_I. (a) Mass fraction of olivine in the residual assemblage as a function of pressure. The dashed line marks the exhaustion of cpx for each value of Ω_I. (b) Mass fractions of opx and cpx in the residual assemblage as functions of pressure. The dashed line marks the modal abundance of opx at the exhaustion of cpx for each value of Ω_I. (c) Apparent melt productivity ($-d\tilde{F}/dP$) vs pressure. As long as the residual assemblage remains the same, ($-d\tilde{F}/dP$) increases monotonically with Ω_I. Productivity drops at the exhaustion of opx and cpx are indicated. (d) Mass fractions of opx and cpx in the residue plotted against $\tilde{F}$ on a reversed scale. For each value of Ω_I, the stoichiometric coefficient of cpx (slope on this diagram) in the melting reaction is roughly constant with respect to $\tilde{F}$ whereas the coefficient of opx increases. Hence as the exhaustion of cpx moves to higher $\tilde{F}$ with increasing Ω_I, less opx remains at the exhaustion of cpx (dashed line).

at pressures above ~1 GPa is limited (Asimow, 1997), so even extreme focusing factors do not produce much melt flux through the column below this level.

The second effect limiting exhaustion of opx to low pressure is that the melt flux required to exhaust opx from peridotites increases with pressure. The minimum $\tilde{F}$ values for exhaustion of opx from the residue (i.e. when opx-out occurs at 1 bar) in the three cases of focusing discussed above (i.e. discrete focusing, cold continuous focusing, and hot continuous focusing) are 0·36, 0·46, and 0·36. Except for the cold continuous focusing case, this value is essentially identical to the melt fraction at which opx is exhausted at 1 bar by adiabatic batch melting of the source composition in the absence of focusing, $F = 0{\cdot}36$ (requiring, according to MELTS, a minimum potential temperature of 1500°C and a solidus deeper than 6 GPa). Batch melting and the various focusing calculations we have done all require higher F (or $\tilde{F}$) to exhaust opx at higher pressure (see Fig. 6c); e.g. the batch melting adiabat that exhausts opx at 0·05 GPa does so at $F = 0{\cdot}37$, whereas the batch melting adiabat that exhausts opx at 0·15 GPa does so at $F = 0{\cdot}40$. The current MELTS calibration, however, tends to overestimate the stability of opx relative to olivine (Hirschmann *et al.*, 1998), and the overstability of opx in MELTS appears to increase with pressure (Asimow, 1997), such that MELTS predicts opx as the liquidus phase (i.e. opx is exhausted at $F = 1$, which is not observed in melting experiments on peridotite at any pressure) for this source composition above ~2·2 GPa. Hence our modeling probably overstates the difficulty of making dunite at high pressure. Nevertheless, the increase in opx stability relative to olivine with increasing pressure is a well-established feature of basaltic phase equilibria (Yoder, 1976; Elthon & Scarfe, 1984), so the increasing difficulty of making dunite residues at higher pressure is correct

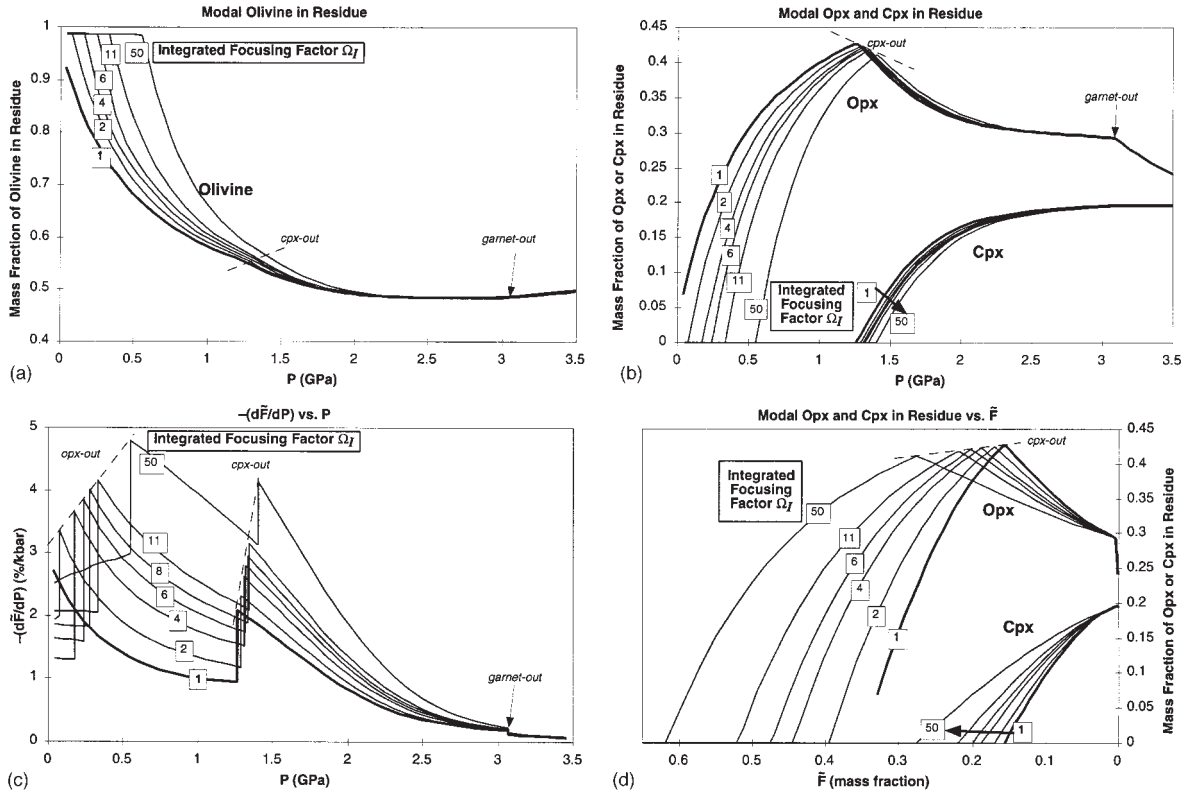

Fig. 5. The effect of continuous focusing of melt into a one-dimensional steady equilibrium porous flow column as in Fig. 4, except this system begins melting at 3·5 GPa, in the garnet peridotite stability field. [Note the changes in productivity and melt reaction stoichiometry at the exhaustion of garnet at 3·1 GPa (spinel is always present, as this composition contains Cr_2O_3 and MELTS does not incorporate this component into solid phases other than spinel).]

in sign if not necessarily in magnitude (i.e. for fixed mineral and bulk compositions, the lever rule requires that as the ol + opx cotectic moves towards an olivine-rich bulk composition, the melt fraction required to exhaust opx increases). The same effect is apparent (although different in magnitude) in the model of Longhi (1992), which for batch melting of this source composition predicts exhaustion of opx at $F = 0{\cdot}3$ at 1 bar, $F = 0{\cdot}4$ at 1 GPa and $F = 0{\cdot}5$ at 3 GPa. Although improvements to MELTS as well as calculations in higher spatial dimensions will be required to establish the relationship between focusing factor and limiting pressure of dunite with certainty, an estimate can be made with the present calculations. We propose as a simple (but approximate) criterion for the minimum focusing factor required to produce a dunite channel by equilibrium porous flow that the melt flux in the channel (expressed as an apparent extent of melting, i.e. melt flux over melt plus solid flux, which is equal to $\tilde{F}$ in the appropriate analogous batch melting column) be greater than or equal to the F needed to exhaust opx by batch melting of the unmodified source composition at the pressure of interest (Fig. 6c). In future revisions of MELTS or in different thermodynamically based models altogether, the value of F at which opx is exhausted by batch melting at a given pressure is likely to change and the relationship between focusing factor and pressure of dunite formation would then change as well. We suggest, however, that this simple approximate criterion will continue to hold; i.e. the batch melting F at which opx is exhausted from the source composition as a function of pressure will remain a minimum for the focused porous flow $\tilde{F}$. Furthermore, the qualitative notion that equilibration between melt and residue at low pressure is necessary to generate replacive dunite is robust: for example, according to MELTS, 'adiabatic fractional' melting [i.e. a series of isentropic upwelling steps followed by extraction of the liquid, removing entropy from the system (Asimow *et al.*, 1995)] cannot exhaust opx from the residue unless the potential temperature is $\geq 1800°C$; even taking into account temperature errors in MELTS, this is much higher than is believed reasonable for upwellings beneath mid-ocean ridges or even 'hotspot' volcanoes (McKenzie & Bickle, 1988; Langmuir *et al.*, 1992).

Discordant dunite veins are observed in the mantle sections of many ophiolite sequences, including the Ho-

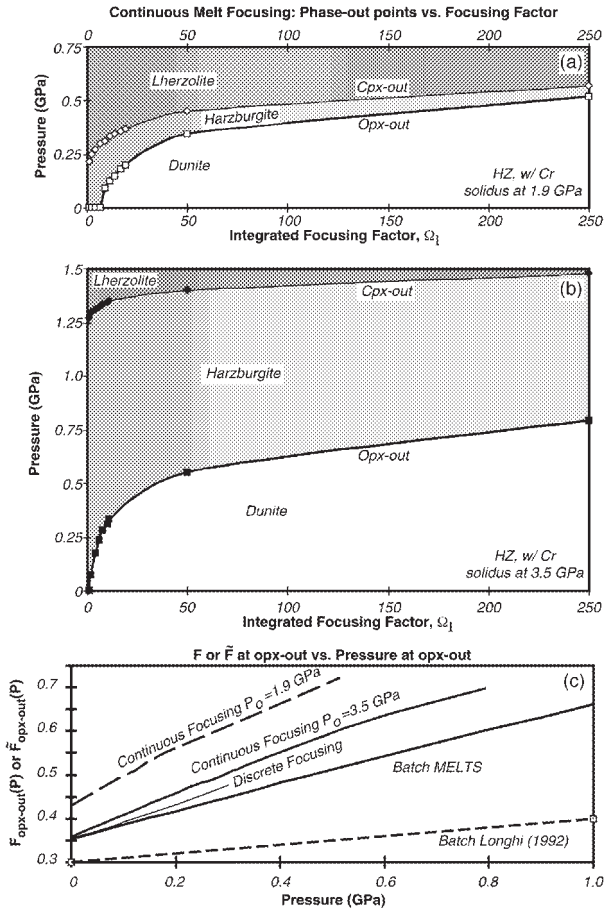

Fig. 6. Summary of the effect of melt focusing on the residual phase assemblage. As a function of integrated focusing factor, Ω_I, the plotted curves for (a) the cold continuous focusing example (1·9 GPa solidus intersection, Fig. 4) and (b) the hot continuous focusing example (3·5 GPa solidus intersection, Fig. 5) divide the residual assemblages into lherzolite (olivine + spinel + opx + cpx), harzburgite (olivine + spinel + opx), and dunite (olivine + spinel) fields. These panels indicate the increase in pressure of cpx-out with increasing Ω_I; the narrowing of the harzburgite field with increasing Ω_I; and the diminishing returns of increasing Ω_I, leading to an approximate limiting pressure for opx-out and cpx-out for each potential temperature. Points on the boundary curves indicate calculations that were performed. (c) Comparison of the apparent extent of melting $\tilde{F}$ in the melt focusing columns (Figs 2, 4, and 5) at the exhaustion of opx as a function of pressure with F at the exhaustion of opx by batch melting of the source composition (Hart & Zindler, 1986) as a function of P. In these examples, focusing always requires $\tilde{F}$ in the melt-enriched composition greater than or equal to $F_{opx\text{-}out}(P)$ for batch melting of the initial source, to exhaust opx and make dunite. Although the steep slopes of all the curves in (c) reflect the overestimate of opx stability relative to olivine in MELTS [compare, e.g. the model of Longhi (1992), short-dashed line], the relationship between the melt focusing curves and the batch melting curve should be robust.

roman peridotite (Takahashi, 1992; Takazawa *et al.*, 1992), the Trinity peridotite (Quick, 1981; Kelemen *et al.*, 1992), the Josephine peridotite (Dick, 1976, 1977; Kelemen & Dick, 1995), and the Oman ophiolite [Kelemen *et al.* (1997) and references therein]. Although other explanations have been advanced to explain these dunites [summarized by Kelemen *et al.* (1995*a*, 1995*b*)], one interpretation is that they formed as channels of focused flow of melt in the mantle (Dick, 1976, 1977; Quick, 1981; Kelemen, 1990; Kelemen & Dick, 1995; Kelemen *et al.*, 1995*a*, 1997), and the results of our modeling provide a framework for understanding the petrological and geochemical consequences of such a process (with the caveat that the assumptions of steady, one-dimensional flow almost certainly do not apply directly to nature). Our results can be used to constrain aspects of the conditions of formation of dunites, including pressure, potential temperature of the source, and melt flux. The pressure of dunite formation is significant because the absence of opx in the conduits of melt migration offers one possible explanation for the observation that liquids parental to MORB are not saturated with opx except at pressures greater than about 0·8 GPa (O'Hara, 1968; Stolper, 1980). MORB is a mixture of liquid increments extracted from a range of mantle conditions, and it is possible to mix liquids each of which are in equilibrium with opx to produce a mixture that is not saturated with opx. If this mixing takes place in the presence of opx, however, the mixture would evolve back to opx saturation. Thus if most mixing of the liquid fractions that contribute to MORB occurs in the mantle before equilibrium with residual phases is lost, observed compositions would suggest that opx is exhausted from the melt flow channels at $P \geq 0{\cdot}8$ GPa. Subject to the uncertainties discussed above, the results presented here imply that this requires both a hot mantle and focusing factors of tens to hundreds. The constraint of high potential temperature in the mantle where an ophiolite was generated (compare Fig. 6a and Fig. 6b; the potential temperature used in Figs 5 and 6b is at the upper end of the range estimated for non-hotspot affected mid-ocean ridges) is in principle testable by observing the extent of depletion of associated harzburgites representing residues of fractional melt extraction. The focusing factors associated with melt flow channels (Fig. 6b) may be related to the areal extent of dunite as a fraction of the mantle section or the size distribution of dunite veins, although it is difficult to reconstruct the geometry at the spreading axis before transposition (Kelemen *et al.*, 1997). It should be noted that in a given one-dimensional equilibrium porous flow column, very little change occurs in the composition of the residue at levels shallower than that at which opx is exhausted. Similarly, there is little difference in the compositions of the dunite residues in columns that differ in the amount of melt focusing. Consequently, as discussed by Kelemen *et al.* (1997), it is difficult to do more than place a lower bound on the melt flux required to produce a dunite vein; further melt flux beyond this point may leave no detectable trace. Our work suggests that these constraints on pressure and

melt flux are in fact correlated: to form a dunite at higher pressure requires a larger minimum melt flux (Fig. 6c).

Petrological and geochemical similarities between natural dunite veins and the model dunites generated by focused flow in MELTS include the forsterite content of the olivine, the rare-earth element (REE) patterns, and the spinel compositions:

(1) the olivine compositions of all the dunite residues produced in these calculations have *mg*-number [i.e. molar Mg/(Mg + Fe)] in the range 0·908–0·910 for the cold continuous and discrete calculations and 0·912–0·919 for the hot continuous calculations, comparable with the range reported in natural dunites in peridotite exposures [0·90 ± 0·01 in the Horoman complex (Takahashi, 1992); 0·895–0·91 in Oman (Kelemen *et al.*, 1995*a*)]. Cumulate dunites, on the other hand, would evolve toward lower forsterite contents if they represented a significant fraction of crystallization, unless the liquid were continually replenished (Kelemen *et al.*, 1997).

(2) As noted by Kelemen *et al.* (1995*a*), the REE patterns of rare cpx grains in natural dunitic veins in ophiolites are consistent with equilibrium with MORB-like liquid, in contrast to cpx grains from peridotites interpreted as residues that have experienced some degree of fractional melting [including abyssal peridotites (Johnson *et al.*, 1990) and Oman harzburgites (Kelemen *et al.*, 1995*a*)], which are extremely depleted in the light REE. We coupled our MELTS calculations to simple trace element fractionation calculations, using mineral partition coefficients from McKenzie & O'Nions (1995) and bulk partition coefficients calculated from the modal mineralogy determined by MELTS. The resulting REE patterns in cpx (reported in Fig. 7a at a common datum of 0·5 GPa, where some cpx remains in the residue of all these calculations; it should be noted, however, that 'fictive' cpx grains calculated to be in REE equilibrium with the liquid present at the base of the crust in each calculation would look nearly identical) from melt focusing calculations and in fractional melting calculations resemble the patterns seen in dunites from Oman and in abyssal peridotites and harzburgites from Oman, respectively. We thus support the interpretation of Kelemen *et al.* (1995*a*) that dunite formation by focused porous flow is consistent with the cpx REE data from Oman (although this does not rule out other possibilities).

(3) The same result emerges from examination of the spinel compositions predicted by our melt focusing calculations (Fig. 7b). Spinel grains in dunites from Oman have high TiO_2 and high *cr*-number [i.e. molar Cr/(Cr + Al)], whereas the spinels in harzburgites from Oman have low TiO_2 and moderate *cr*-number (Kelemen *et al.*, 1995*a*), and spinels in abyssal peridotites (excepting plagioclase-bearing samples) have a broad range of *cr*-number but reproducibly low TiO_2 (Dick & Bullen, 1984). In Fig. 7b, continuous melt focusing calculations (see Figs 4 and 5) at two potential temperatures and with a range of focusing factors, Ω_l, produce residual spinels that evolve to high *cr*-number with increasing $\tilde{F}$ while maintaining roughly constant TiO_2. The spinel paths enter the field of natural dunites near the point where opx is exhausted from the calculated residues, although spinels in harzburgites produced by equilibrium porous flow without focusing (i.e. $\Omega_l = 1$) also plot in this field. Fractional melting calculations at the same two potential temperatures produce residual spinels that evolve at high extents of melting to low TiO_2 and moderate *cr*-number, consistent with the compositions of spinels in Oman harzburgites and abyssal peridotites interpreted as residues of fractional melting. The spinel compositions in the model dunite and harzburgites are not consistent with trends observed in the Horoman peridotite (Takahashi, 1992), where dunites interpreted as cumulate in origin have lower *cr*-number than associated harzburgites.

All three of these similarities demonstrate essentially that both natural and model dunites are in equilibrium with MORB-like liquid. It should be noted that these similarities do not constrain the presence or extent of focusing; they only demonstrate that the focusing hypothesis is consistent with the characteristics of natural dunites. From the standpoint of our calculations, it is the mineralogy of the dunites (rather than the olivine *mg*-number content, REE patterns, or spinel compositions) that requires focusing. Although the ability of the steady, one-dimensional melt focusing model to account for the observed features of dunites in some ophiolites does not prove that the natural dunites are produced by comparable processes (or, by extension, that the constraints derived on conditions of dunite formation are relevant to natural dunites), they do nevertheless demonstrate that melt focusing is a reasonable explanation for the formation of these veins, as championed by Dick (1976, 1977; Dick & Bullen, 1984), Quick (1981), Kelemen (1990; Kelemen & Dick, 1995; Kelemen *et al.*, 1995*a*, 1997) and others. Moreover, in the context of such models, the conditions (e.g. the minimum melt flux) required to form dunite are also consistent with aspects of the geochemical characteristics of at least some natural dunites.

CONCLUSIONS

In the absence of diffusion, a one-dimensional upwelling column of partially melting mantle undergoing steady-state, equilibrium porous flow is required by conservation of mass to yield melt and residue compositions at each point in the column identical to those attained by batch melting of the source composition at the same P and T (or any combination of P, T, and F taken two at a time). Except for dissipative source terms for solid compaction

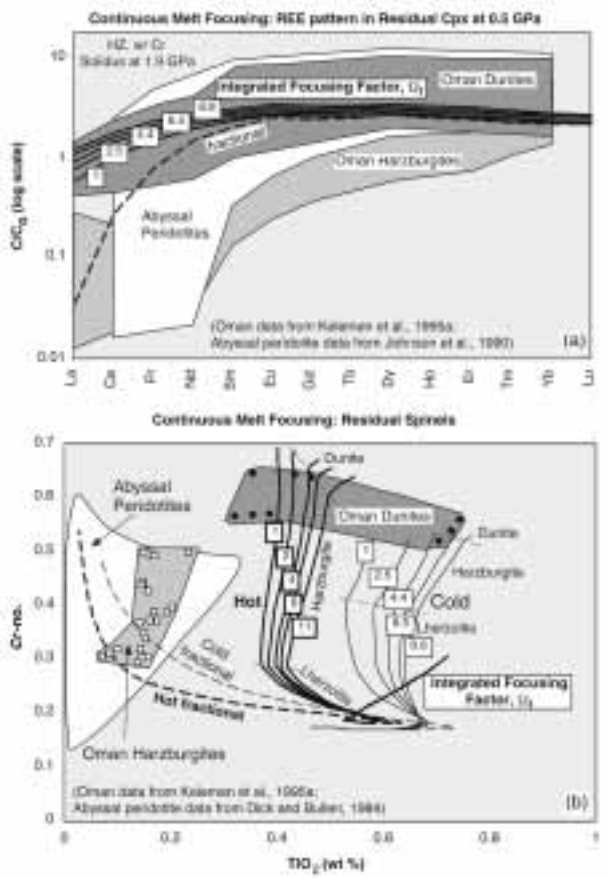

Fig. 7. Comparison of model solid compositions generated by continuous melt focusing (see text and Figs 4 and 5) and model residues of fractional melting with natural dunites and harzburgites interpreted to represent melt focusing conduits and fractional melting residues, respectively. (a) Rare-earth element (REE) patterns in the residual cpx at 0·5 GPa for the cold continuous focusing calculations (Fig. 4) and for an incrementally isentropic fractional fusion calculation with the same potential temperature, compared with the range of REE patterns in cpx grains in dunites and harzburgites from Oman (Kelemen *et al.*, 1995*a*) and abyssal peridotites (Johnson *et al.*, 1990). The model cpx calculated for continuous focusing represents a good match to the Oman dunites, whereas the fractional melting residues match best the abyssal peridotites and Oman harzburgites. (b) *cr*-number [molar Cr/(Cr + Al)] vs TiO_2 (wt %) of spinels. The numbered curves show evolution of the residues as functions of pressure in the continuous focusing columns ('Cold' refers to solidus at 1·9 GPa as in Fig. 4; 'Hot' refers to solidus at 3·5 GPa as in Fig. 5); for the focusing calculations the light dashed lines divide the paths into lherzolite, harzburgite, and dunite fields. The near-horizontal segment at the beginning of the 'Cold' batch and fractional paths transits the near-solidus region where the partitioning behavior of Ti is changing rapidly (Baker & Stolper, 1994; Baker *et al.*, 1995); the positively sloped diagonal segment at the beginning of the 'Hot' batch and fractional paths (all superimposed) occupies the garnet–spinel peridotite transition where Al is added to spinel by decomposition of garnet. Oman ophiolite data from Kelemen *et al.* (1995*a*). Abyssal peridotite data from Dick & Bullen (1984). The Oman harzburgites, interpreted as residues of fractional melting, have moderate *cr*-number and low TiO_2; abyssal peridotites, although more scattered, overlap the same region. The model fractional melting residues also pass into this field at moderate extents of melting. The Oman dunites, interpreted as channels of focused flow, have high *cr*-number and high TiO_2; the model focusing paths reach this field near the transition to dunite.

and gravity, energy conservation similarly requires the temperature and extent of melting at any pressure to equal those achieved by isentropic closed-system upwelling (i.e. isentropic batch melting). This analogy between steady one-dimensional melt transport and batch melting allows some simple calculations of melt migration phenomena.

When melt flow is focused into a channel but maintains equilibrium with the residue in the channel, then compared with simple steady-state, one-dimensional flow without focusing, at a given depth shallower than the focusing event, this is equivalent to batch melting of increasingly fertile bulk compositions at higher extents of melting. Both the increased fertility and higher extents of melting contribute to higher melt productivity ($-dF/dP$), and a larger coefficient for opx in the melting reaction and hence faster removal of opx from the residue. Consequently, even a relatively small amount of melt focusing can produce a dunite residue if melting continues to 1 bar, whereas typical mantle undergoing fractional or batch fusion without focusing cannot produce such a residue. Generating a dunite at higher pressure, however, requires a larger minimum melt flux; a dunite residue at pressures near 1 GPa requires a combination of anomalously high mantle potential temperature and high focusing factors ($>10^2$). The dunites generated by this focusing mechanism have olivine and spinel compositions and REE patterns similar to those of natural dunites observed in some ophiolite sequences.

ACKNOWLEDGEMENTS

The authors thank Tim Elliott, Peter Reiners and Marc Spiegelman for careful and thoughtful reviews, and Jon Davidson for editorial handling. John Longhi kindly performed some calculations for us with his melting model. We have had numerous helpful discussions with Peter Kelemen and Marc Spiegelman. This work was supported by NSF Grants OCE-9529878 and EAR-9219899, and by a Lamont–Doherty Earth Observatory postdoctoral fellowship to P.D.A. This is Caltech Division of Geological and Planetary Sciences Contribution 8508.

REFERENCES

Aharonov, E., Whitehead, J. A., Kelemen, P. B. & Spiegelman, M. (1995). Channeling instability of upwelling melt in the mantle. *Journal of Geophysical Research* **100,** 20433–20450.

Ahern, J. L. & Turcotte, D. L. (1979). Magma migration beneath an ocean ridge. *Earth and Planetary Science Letters* **45,** 115–122.

Asimow, P. D. (1997). A thermodynamic model of adiabatic melting of the mantle. Ph.D. Thesis, California Institute of Technology, Pasadena.

Asimow, P. D., Hirschmann, M. M., Ghiorso, M. S., O'Hara, M. J. & Stolper, E. M. (1995). The effect of pressure-induced solid–solid

phase transitions on decompression melting of the mantle. *Geochimica et Cosmochimica Acta* **59,** 4489–4506.

Asimow, P. D., Hirschmann, M. M. & Stolper, E. M. (1997). An analysis of variations in isentropic melt productivity. *Philosophical Transactions of the Royal Society of London, Series A* **355,** 255–281.

Baker, M. B. & Stolper, E. M. (1994). Determining the composition of high-pressure mantle melts using diamond aggregates. *Geochimica et Cosmochimica Acta* **58,** 2811–2827.

Baker, M. B., Hirschmann, M. M., Ghiorso, M. S. & Stolper, E. M. (1995). Compositions of low-degree partial melts of peridotite: results from experiments and thermodynamic calculations. *Nature* **375,** 308–311.

Condomines, M., Morand, P. & Allègre, C. J. (1981). ^{230}Th–^{238}U disequilibria in oceanic tholeiites from 21°N on the East Pacific Rise. *Earth and Planetary Science Letters* **55,** 393–406.

Dick, H. J. B. (1976). The origin and emplacement of the Josephine peridotite of Southwestern Oregon. Ph.D. Thesis, Yale University, New Haven, CT.

Dick, H. J. B. (1977). Evidence for partial melting in the Josephine peridotite. *Bulletin of the Oregon State Department of Geology and Mineral Industries* **96,** 63–78.

Dick, H. J. B. & Bullen, T. (1984). Chromian spinel as a petrogenetic indicator in abyssal and alpine-type peridotites and spatially associated lavas. *Contributions to Mineralogy and Petrology* **86,** 54–76.

Elthon, D. & Scarfe, C. M. (1984). High-pressure phase equilibria of a high-magnesia basalt and the genesis of primary oceanic basalts. *American Mineralogist* **69,** 1–15.

Ghiorso, M. S. (1994). Algorithms for the estimation of phase stability in heterogeneous thermodynamic systems. *Geochimica et Cosmochimica Acta* **58,** 5489–5501.

Ghiorso, M. S. & Sack, R. O. (1995). Chemical mass transfer in magmatic processes IV. A revised and internally consistent thermodynamic model for the interpolation and extrapolation of liquid–solid equilibria in magmatic systems at elevated temperatures and pressures. *Contributions to Mineralogy and Petrology* **119,** 197–212.

Hart, S. R. (1993). Equilibration during mantle melting: a fractal tree model. *Proceedings of the National Academy of Science* **90,** 11914–11918.

Hart, S. R. & Zindler, A. (1986). In search of a bulk-earth composition. *Chemical Geology* **57,** 247–267.

Hess, P. C. (1992). Phase equilibria constraints on the origin of ocean floor basalt. In: Phipps Morgan, J., Blackman, D. K. & Sinton, J. M. (eds) *Mantle Flow and Melt Generation at Mid-Ocean Ridges. Geophysical Monograph, American Geophysical Union* **71,** 67–102.

Hirschmann, M. M., Stolper, E. M. & Ghiorso, M. S. (1994). Perspectives on shallow mantle melting from thermodynamic calculations. *Mineralogical Magazine* **58A,** 418–419.

Hirschmann, M. M., Ghiorso, M. S., Wasylenki, L. E., Asimow, P. D. & Stolper, E. M. (1998). Calculation of peridotite partial melting from thermodynamic models of minerals and melts. I. Methods and comparison to experiments. *Journal of Petrology* **39,** 1091–1115.

Hirschmann, M. M., Asimow, P. D., Ghiorso, M. S. & Stolper, E. M. (1999). Calculation of peridotite partial melting from thermodynamic models of minerals and melts. III. Controls on isobaric melt production and the effect of water on melt production. *Journal of Petrology* (in press).

Johnson, K. T. M., Dick, H. J. B. & Shimizu, N. (1990). Melting in the oceanic upper mantle: an ion microprobe study of diopsides in abyssal peridotites. *Journal of Geophysical Research* **95,** 2661–2678.

Kelemen, P. B. (1986). Assimilation of ultramafic rock in subduction-related magmatic arcs. *Journal of Geology* **94,** 829–843.

Kelemen, P. B. (1990). Reaction between ultramafic rock and fractionating basaltic magma I. Phase relations, the origin of calc-alkaline magma series, and the formation of discordant dunite. *Journal of Petrology* **31,** 51–98.

Kelemen, P. B. & Dick, H. J. B. (1995). Focused melt flow and localized deformation in the upper mantle: juxtaposition of replacive dunite and ductile shear zones in the Josephine peridotite, SW Oregon. *Journal of Geophysical Research* **100,** 423–438.

Kelemen, P. B. & Ghiorso, M. S. (1986). Assimilation of peridotite in zoned calc-alkaline plutonic complexes: evidence from the Big Jim complex, Washington Cascades. *Contributions to Mineralogy and Petrology* **94,** 12–28.

Kelemen, P. B., Dick, H. J. B. & Quick, J. E. (1992). Formation of harzburgite by pervasive melt/rock reaction in the upper mantle. *Nature* **358,** 635–641.

Kelemen, P. B., Shimizu, N. & Salters, V. J. M. (1995*a*). Extraction of mid-ocean-ridge basalt from the mantle by focused flow of melt in dunite channels. *Nature* **375,** 747–753.

Kelemen, P. B., Whitehead, J. A., Aharonov, E. & Jordahl, K. A. (1995*b*). Experiments on flow focusing in soluble porous media, with applications to melt extraction from the mantle. *Journal of Geophysical Research* **100,** 475–496.

Kelemen, P. B., Hirth, G., Shimizu, N., Spiegelman, M. & Dick, H. J. B. (1997). A review of melt migration processes in the adiabatically upwelling mantle beneath oceanic spreading ridges. *Philosophical Transactions of the Royal Society of London, Series A* **355,** 283–318.

Kinzler, R. J. & Grove, T. L. (1992). Primary magmas of mid-ocean ridge basalts 2. Applications. *Journal of Geophysical Research* **97,** 6907–6926.

Klein, E. M. & Langmuir, C. H. (1987). Global correlations of ocean ridge basalt chemistry with axial depth and crustal thickness. *Journal of Geophysical Research* **92,** 8089–8115.

Kohlstedt, D. L. (1991). Structure, rheology, and permeability of partially molten rocks at low melt fractions. In: Phipps Morgan, J., Blackman, D. K. & Sinton, J. M. (eds) *Mantle Flow and Melt Generation at Mid-Ocean Ridges. Geophysical Monograph, American Geophysical Union* **71,** 103–122.

Langmuir, C. H., Klein, E. M. & Plank, T. (1992). Petrological systematics of mid-ocean ridge basalts: constraints on melt generation beneath ocean ridges. In: Phipps Morgan, J., Blackman, D. K. & Sinton, J. M. (eds) *Mantle Flow and Melt Generation at Mid-Ocean Ridges. Geophysical Monograph, American Geophysical Union* **71,** 183–280.

Longhi, J. (1992). Origin of green glass magmas by polybaric fractional fusion. *Proceedings in Lunar and Planetary Sciences* **22,** 343–353.

McKenzie, D. P. (1984). The generation and compaction of partial melts. *Journal of Petrology* **25,** 713–765.

McKenzie, D. P. & Bickle, M. J. (1988). The volume and composition of melt generated by extension of the lithosphere. *Journal of Petrology* **29,** 625–679.

McKenzie, D. P. & O'Nions, R. K. (1995). The source regions of ocean island basalts. *Journal of Petrology* **36,** 133–159.

Navon, O. & Stolper, E. M. (1987). Geochemical consequences of melt percolation—the upper mantle as a chromatographic column. *Journal of Geology* **95,** 285–307.

Newman, S., Finkel, R. C. & MacDougall, J. D. (1983). ^{230}Th–^{238}U disequilibrium systematics in oceanic tholeiites from 21°N on the East Pacific Rise. *Earth and Planetary Science Letters* **65,** 17–33.

Niu, Y. & Batiza, R. (1991). An empirical method for calculating melt compositions produced beneath mid-ocean ridges: application to axis and off-axis (seamounts) melting. *Journal of Geophysical Research* **96,** 21753–21777.

O'Hara, M. J. (1968). Are ocean floor basalts primary magmas? *Nature* **220,** 683–686.

Parmentier, E. M. & Phipps Morgan, J. (1990). Spreading rate dependence of three-dimensional structure in oceanic spreading centers. *Nature* **348,** 325–328.

Phipps Morgan, J. (1987). Melt migration beneath mid-ocean ridge spreading centers. *Geophysical Research Letters* **14,** 1238–1241.

Phipps Morgan, J. & Forsyth, D. W. (1988). Three-dimensional flow and temperature perturbations due to a transform offset: effects on oceanic crustal and upper mantle structure. *Journal of Geophysical Research* **93,** 2955–2966.

Quick, J. E. (1981). The origin and significance of large tabular dunite bodies in the Trinity peridotite, Northern California. *Contributions to Mineralogy and Petrology* **78,** 413–422.

Reinitz, I. & Turekian, K. K. (1989). $^{230}Th/^{238}U$ and $^{226}Ra/^{230}Th$ fractionation in young basaltic glasses from the East Pacific Rise. *Earth and Planetary Science Letters* **94,** 199–207.

Ribe, N. M. (1985). The generation and composition of partial melts in the earth's mantle. *Earth and Planetary Science Letters* **73,** 361–376.

Richter, F. M. (1986). Simple models for trace element fractionation during melt segregation. *Earth and Planetary Science Letters* **77,** 333–344.

Richter, F. M. & McKenzie, D. P. (1984). Dynamical models for melt segregation from a deformable matrix. *Journal of Geology* **92,** 729–740.

Scott, D. R. (1992). Small-scale convection and mantle melting beneath mid-ocean ridges. In: Phipps Morgan, J., Blackman, D. K. & Sinton, J. M. (eds) *Mantle Flow and Melt Generation at Mid-Ocean Ridges. Geophysical Monograph, American Geophysical Union* **71,** 327–352.

Scott, D. R. & Stevenson, D. J. (1984). Magma solitons. *Geophysical Research Letters* **11,** 1161–1164.

Scott, D. R. & Stevenson, D. J. (1989). A self-consistent model of melting, magma migration and buoyancy-driven circulation beneath mid-ocean ridges. *Journal of Geophysical Research* **94,** 2973–2988.

Sleep, N. H. (1988). Tapping of melt by veins and dikes. *Journal of Geophysical Research* **93,** 10255–10272.

Sparks, D. W. & Parmentier, E. M. (1993). The structure of three-dimensional convection beneath oceanic spreading centers. *Geophysical Journal International* **112,** 81–91.

Spiegelman, M. (1993*a*). Flow in deformable porous media. Part 1: Simple analysis. *Journal of Fluid Mechanics* **247,** 17–38.

Spiegelman, M. (1993*b*). Flow in deformable porous media. Part 2: Numerical analysis—the relationship between shock waves and solitary waves. *Journal of Fluid Mechanics* **247,** 39–63.

Spiegelman, M. (1996). Geochemical consequences of melt transport in 2-D: the sensitivity of trace elements to mantle dynamics. *Earth and Planetary Science Letters* **139,** 115–132.

Spiegelman, M. & Elliott, T. (1993). Consequences of melt transport for uranium series disequilibrium in young lavas. *Earth and Planetary Science Letters* **118,** 1–20.

Spiegelman, M. & Kenyon, P. (1992). The requirements for chemical disequilibrium during magma migration. *Earth and Planetary Science Letters* **109,** 611–620.

Spiegelman, M. & McKenzie, D. (1987). Simple 2-D models for melt extraction at mid-ocean ridges and island arcs. *Earth and Planetary Science Letters* **83,** 137–152.

Stevenson, D. J. (1989). Spontaneous small-scale melt segregation in partial melts undergoing deformation. *Geophysical Research Letters* **16,** 1067–1070.

Stevenson, D. J. & Scott, D. R. (1991). Mechanics of fluid–rock systems. *Annual Reviews of Fluid Mechanics* **23,** 305–339.

Stolper, E. M. (1980). A phase diagram for mid-ocean ridge basalts. *Contributions to Mineralogy and Petrology* **74,** 13–27.

Takahashi, N. (1992). Evidence for melt segregation towards fractures in the Horoman mantle peridotite complex. *Nature* **359,** 52–55.

Takazawa, E., Frey, F. A., Shimizu, N., Obata, M. & Bodinier, J. L. (1992). Geochemical evidence for melt migration and reaction in the upper mantle. *Nature* **359,** 55–58.

Turcotte, D. L. & Ahern, J. L. (1978). A porous flow model for magma migration in the asthenosphere. *Journal of Geophysical Research* **83,** 767–772.

von Bargen, N. & Waff, H. S. (1986). Permeabilities, interfacial areas and curvatures of partially molten systems: results of numerical computations of equilibrium microstructures. *Journal of Geophysical Research* **91,** 9261–9276.

Waff, H. S. & Bulau, J. R. (1979). Equilibrium fluid distribution in an ultramafic partial melt under hydrostatic stress conditions. *Journal of Geophysical Research* **84,** 6109–6114.

Yoder, H. S. (1976). *Generation of Basaltic Magma.* Washington, DC: National Academy of Sciences, pp. 143–144.